Materials Science & Engineering C 88 (2018) 115–129

Contents lists available at ScienceDirect

Materials Science & Engineering C

journal homepage: www.elsevier.com/locate/msec

Zinc and nitrogen ornamented bluish white luminescent carbon dots for engrossing bacteriostatic activity and Fenton based bio-sensor

Poushali Das[a], Sayan Ganguly[b], Madhuparna Bose[c], Subhadip Mondal[b], Sumita Choudhary[d], Subhashis Gangopadhyay[d], Amit Kumar Das[c], Susanta Banerjee[e], Narayan Chandra Das[a,b,*]

[a] School of Nanoscience and Technology, Indian Institute of Technology, Kharagpur 721302, India
[b] Rubber Technology Centre, Indian Institute of Technology, Kharagpur 721302, India
[c] Department of Biotechnology, Indian Institute of Technology, Kharagpur 721302, India
[d] Department of Physics, Birla Institute of Technology & Science, Pilani, Rajasthan 333031, India
[e] Materials Science Centre, Indian Institute of Technology, Kharagpur 721302, India

ABSTRACT

Carbon dots with heteroatom co-doping associated with consummate luminescence features are of acute interest in diverse applications such as biomolecule markers, chemical sensing, photovoltaic, and trace element detection. Herein, we demonstrate a straightforward, highly efficient hydrothermal dehydration technique to synthesize zinc and nitrogen co-doped multifunctional carbon dots (N, Zn-CDs) with superior quantum yield (50.8%). The luminescence property of the carbon dots can be tuned by regulating precursor ratio and surface oxidation states in the carbon dots. A unique attribution of the as-prepared carbon dots is the high monodispersity and robust excitation-independent emission behavior that is stable in enormously reactive environment and over a wide range of pH. These N, Zn-CDs unveils captivating bacteriostatic activity against gram-negative bacteria *Escherichia coli*. Furthermore, the excellent luminescence properties of these carbon dots were applied as a platform of sensitive biosensor for the detection of hydrogen peroxide. Under optimized conditions, these N, Zn-CDs reveals high sensitivity over a broad range of concentrations with an ultra-low limit of detection (LOD) indicating their pronounced prospective as a fluorescent probe for chemical sensing. Overall, the experimental outcomes propose that these zero-dimensional nano-dots could be developed as bacteriostatic agents to control and prevent the persistence and spreading of bacterial infections and as a fluorescent probe for hydrogen peroxide detection.

1. Introduction

In recent era, with the astonishing advances of nanotechnology, nanoparticles with distinct physical and chemical properties have revealed an increasing significance in biomedical, biological, and pharmaceutical applications [1,2]. Owing to the advancement in science and technology it has become possible to fabricate, characterize and tailor the functional properties of the nanoparticles for their applications in different fields. With the rapid developments in fluorescence spectroscopy and microscopy, fluorescent materials have become more significant than ever for several applications such as sensors, healthcare and biomedical applications [3–8]. Also, fluorescent nanoparticles based probe have emerged as a promising platform for a variety of biological applications. For instance, Xian Jun Loh and his coworkers demonstrated luminescent upconversion material for bioimaging and biodetection techniques. They examined the recent developments in the field of luminescent upconversion material in the mechanics of TTA (Triplet–triplet annihilation) with reference to the applicability in biomedical fields [9]. A group of scientist developed efficient gene delivery platform to mouse embryonic stem cell colonies which is reported elsewhere [10]. Among different types of nanoparticles zero dimensional carbon dots (CDs), a newcomer to the globe of nanolights and nanomaterials have fascinated growing attention due to their interesting properties of sensor design, excellent biocompatibility, medical diagnosis, low toxicity, photocatalysts, tunable luminescence property, antibacterial properties and also being potential building blocks for nanodevices [11–18]. Being photoactive CDs are nonblinking and photochemically and physicochemically stable [19,20]. Due to these characteristic features they became popular in the ground of multicolor and one or two photon in bio-imaging of in vitro and in vivo [21,22]. Besides, attributing to their ample surface oxygen functionalities and hydrophilicity, CDs have been acknowledged as an auspicious

* Corresponding author at: School of Nanoscience and Technology, Indian Institute of Technology, Kharagpur 721302, India.
E-mail address: ncdas@rtc.iitkgp.ernet.in (N.C. Das).

https://doi.org/10.1016/j.msec.2018.03.010
Received 2 August 2017; Received in revised form 14 September 2017; Accepted 14 March 2018
Available online 15 March 2018
0928-4931/

support for construction of optical sensor for environmental pollutants and quantitative assay of biomolecules [23,24]. Their remarkable properties like robustness against photobleaching, optical absorptivity, chemical inertness, ease of functionalization, good adaptability as well as low cost augment their applicability under sundry conditions [25–30]. But, the great challenge concerning the utilization of pristine CDs is the moderate quantum yield with modest luminescence properties unveiled by intrinsic CDs. Numerous approaches including functionalization, heteroatom doping [31], surface passivation were generated to boost their photoluminescence properties and modification of CDs. Among these techniques, heteroatom doping have captured substantial attention of the scholars around the world owing to their facile nature as well as cost effectiveness [32–35]. For example, a simple hydrothermal method was reported by Yang et al. to prepare nitrogen doped CDs using citric acid and ethylenediamine with very high QY (80%) [36]. This high QY value is nearly equivalent to that of fluorescent dyes. Xu et al. reported a slimplistic way to prepare sulfur doped CDs by using sodium citrate and sodium thiosulfate [37]. Dopants like boron (B) [38], phosphorus (P) [39], silicon (Si) [33] have also been incorporated to embellish the luminescence properties of the CDs. Moreover to single heteroatom doping strategy, co-heteroatom doping approach had been also studied due to the synergistic effect between the doped heteroatoms appears to be quite beneficial. For instance, Yu et al. reported similar hydrothermal approach to synthesize sulfur and nitrogen co-doped CDs with L-cysteine and citric acid as precursors, which shows 73% QY [40].

Incorporation of metal atoms into the CDs matrix has found little advancement, comparison to the non-metal doping approach. Wu et al. reported improved electron-donating and accepting ability by co-doping the CDs with nitrogen and copper and applied them as a promising photocatalyst application [41]. Nevertheless, introduction of metal atom into CDs matrix is associated with increase toxicity. Therefore, ideal dopant metal should not provide toxicity to the CDs and also should be ecologically benign. Zinc (Zn) is a vital element assisting numerous electron transfer processes in environment. It is also a trace element for different bio-systems. It has been reported that Zn has negligible toxic character. Zn deficiency causes many health hazards. Therefore, usage of Zn as dopant into the CDs matrix is quite beneficial to enhance the properties of these zero dimensional tiny nanomaterial. In this context, incorporation of Zn has illustrated improvement of different properties, previously. Guo et al. described that the performance of photodetectors could considerably increase with the introduction of zinc oxide quantum dots/carbon nanodots hybrid films [42]. Zhang et al. reported sol-gel method to prepare ZnO/carbon quantum dot which showed an excellent photocatalytic activity [43]. Zinc doped CDs (QY 29.3%) obtained from chitosan/metal ion complex was reported by Li and his co-workers [44].

Moreover, the antibacterial activity of zinc oxide (ZnO) nanoparticles has been investigated with various non-pathogenic and pathogenic bacteria like *E. coli* and *S. aureus* [45–48]. ZnO nanoparticles are biosafe, non-toxic, biocompatible and have application in the field of drug carrier, filling in medical materials, cosmetic [49]. Previously many studies have shown the harmful effect of nanomaterials on live cells but very low concentrations of ZnO are non-toxic to eukaryotic cells [50,51]. ZnO with a wide band gap of 3.37 eV displayed a good photocatalytic activity. Various methods to prepare ZnO CDs with photocatalytic features had been reported previously. A nice overlap was found between the photoluminescence range of CDs and ZnO. Hence, there is a possibility of energy/charge transfer between CDs and ZnO due to this overlap.

Herein, we report a facile pathway to synthesized bluish white luminescence nitrogen and zinc co-doped CDs (N, Zn-CDs) with high quantum yield (QY) > 50%. These heteroatom co-doped CDs exhibits high doping efficiency comparison to other reported studies. The N, Zn-CDs were analyzed for bacteriostatic effect of gram-negative bacteria which is one of the most major foodborne pathogen in food industry. Foods of different origins, including radish sprouts, spinach, pea salad, lettuce, alfalfa, cantaloupe, raw milk, apple cider, mayonnaise, undercooked beef were associated with illnesses caused by these bacteria can give rise to critical diseases like abdominal pain with bloody stools, diarrhoea, colon inflammation etc. The as-prepared N, Zn-CDs exhibits excellent bacteriostatic effect at a very low concentration. Therefore, they can be used in plastics to prevent bacterial growth on surfaces. Moreover, N, Zn-CDs were investigated as fluorescent nano-probe for the H_2O_2 detection grounded on Fenton reaction. The facile synthesis of robust N, Zn-CDs with enhanced luminescence is anticipated to capture widespread attention and applicability.

2. Experimentals

2.1. Materials

Citric acid, tris(hydroxymethyl)aminomethane, ferrous sulfate heptahydrate, hydrogen peroxide and phosphate-buffered saline (PBS) were purchased from Sigma-Aldrich, Germany. Zinc acetate [$(Zn(O_2CCH_3)_2(H_2O)_2$] was purchased from Merck, India. Luria-Bertani (LB) broth was purchased from Himedia, India. *Escherichia coli* (DH5α) used in this experiment were obtained from Department of Biotechnology, Indian Institute of Technology, Kharagpur. All other chemicals used were of reagent grade.

2.2. Synthesis of control CDs and Zn-doped CDs (N, Zn-CDs)

Control CDs (without Zn doping) were synthesized using simple hydrothermal method. Briefly, 25 mL citric acid solution (0.1 M) and tris(hydroxymethyl)aminomethane (0.3 M) were added into a 50 mL poly(tetrafluoroethylene) (Teflon)-lined autoclave. The temperature of the autoclave was kept fixed temperature at 200 °C for 4 h. After the reaction was over, the autoclave was naturally cooled down to room temperature. The obtained pale yellow product was centrifuged at 10000 rpm for 20 min to remove large particles and the supernatant was collected. At last, powdered sample was derived after dialysis and lyophilization. After that, Zn-doped CDs (N, Zn-CDs) was prepared using 25 mL of 0.1 M control CDs solution and 0.05 M zinc acetate. The mixture was transferred to dried poly(tetrafluoroethylene) (Teflon)-lined autoclave and kept at 200 °C for 4 h. The same process was used to carry out solid sample.

2.3. Characterization

The microstructure and morphology of the N, Zn-CDs were investigated using a high resolution transmission electron microscope HRTEM (JEOL, Japan operating voltage 200 kV with filament LaB6). The Fourier transform infrared (FTIR) spectrum of the N, Zn-CDs were recorded on a FTIR spectrophotometer (Perkin Elmer, model-Spectrum-2, Singapore) in the range of 500–4000 cm^{-1} with resolution of 4 cm^{-1} and 16 scans. Scanning electron microscopy (SEM) images of *Escherichia coli* were observed by using FESEM (Field emission Scanning Electron Microscope, MERLIN with Tungsten filament; Carl ZEISS, SMT, Germany) with the accelerating voltage set to 15 kV. The amorphous nature of the N, Zn-CDs were obtained by X-ray Diffractometer (PANalytical High Resolution XRD-I, PW 3040/60). UV–visible absorption spectrum of the prepared N, Zn-CDs in aqueous solution was performed using a UV Spectrometer (PerkinElmer, model-2 Singapore, Lambda35). Fluorescence measurements were measured on a Fluoromax_4C_1052D_4312_FM spectrofluorometer in aqueous dispersion. The fluorescence lifetime was measured at room temperature using a diode laser (Model EPL 375, Edinburg Instruments, Life Spec II) of wavelength 376.6 nm. The elemental composition and mapping of the prepared N, Zn-CDs were analyzed by energy dispersive X-ray study (EDX, INCA PentaFET ×3, Oxford Instrument UK. X-ray photoelectron spectroscopy (XPS) analysis was carried out using a commercial

Omicron EA 125 spectrometer with Al-Kα radiation (1486.7 eV). For all measurements, emission current of the X-ray source was fixed at 20 mA for an anode voltage of 15 kV. XPS samples were prepared by spreading the powder sample on a conducting copper tape. To remove the surface contamination occurred, samples were locally sputter-cleaned using low energy argon ions under the ultra-high vacuum condition prior to the XPS measurements. At the same time, Ar^+ beam induced any kind of degradation of the samples has been eliminated by comparing the XPS spectra before and after the sputter cleaning. High resolution XPS spectra were collected using a pass energy of 20 eV, with a step size of 0.02 eV. The UHV chamber base pressure was maintained $< 10^{-9}$ mbar throughout the measurements. To compensate any kind of charging effect, O 1s binding energy peak at 532.5 eV has been used as a reference here. Using tetramethylsilane (TMS) as an internal standard ^1H NMR was measured in on a Bruker, 600 MHz instrument at ambient temperature. The zeta potential was recorded on a Zetasizer Nano ZS90 (Malvern Instruments, Manchester, U.K.) Raman experiment was carried out using spectrometer (MODEL T64000 (Make JobinYvon Horiba, France). Argon-Krypton mixed ion gas laser (MODEL 2018 RM) was used as an excitation source. Thermoelectric cooled front illuminated 1024 256 CCD, MODEL Synpse TM (Make JobinYvon Horiba, France) was used as the detector.

2.4. Determination of fluorescence quantum yield analysis

Generally, quantum yield is measured relative to an optically dilute standard fluorophore solution which shows a well-known quantum yield (Φ_s). The quantum yield value of unknown fluorophore (Φ_u) was determined using the Parker-Rees method [52,53]. The quantum yield (QY) of the N, Zn-CDs was determined by measuring the fluorescence intensity in aqueous solution. The QY values were calculated using the following equation:

$$\Phi_u = \Phi_s(Y_u/Y_s)(A_s/A_u)(n^2{}_u/n^2{}_s) \quad (1)$$

where Φ is QY value, Y refers to measured integrated fluorescence emission intensity, A corresponds to absorbance measured at the excitation wavelength, n is the refractive index. The subscript “s” corresponds to the standard. The subscript “u” refers to the unknown QY of N, Zn-CDs. In our study, quinine sulfate in 0.1 M H_2SO_4 solution is chosen as standard (literature value of quantum yield 54%).

2.5. Bacterial growth

The Gram-negative *E. coli* cells were cultured in sterile clean room. All the equipments for the *E. coli* cell culture were sterilized at high pressure and high temperature in an autoclave. The culture of *E. coli* was carried out in sterile Luria–Bertani (LB) media (containing 1.0 g bacto-yeast extract, 2.0 g bacto-tryptone and 1.0 g NaCl in 200 mL deionized water). The bacteria cell cultures were grown at 37 °C in an incubator-shaker. After the overnight shaking, 1 mL culture media was centrifuged at 10000 rpm for 10 min to discard the supernatant and washed with PBS buffer and was suspended in 1 mL of PBS buffer.

2.6. Cytotoxicity study

The bacterial cultures were diluted in fresh TSB (tryptone soy broth) starting at an OD at 600 nm (OD_{600}) of 0.05 and incubated at 37 °C overnight in Erlenmeyer flasks as well as on TSA plates. To assess the effect of N, Zn-CDs on *E. coli* cells, the bacterial culture was inoculated by spreading on TSA plates containing different concentrations of N, Zn-CDs (0, 0.2, 0.5, 1 mg/mL), incubated overnight at 37 °C. The inoculated bacterial cells were estimated to be *c*. 200 CFU per plate and all the measurements were performed in triplicate.

2.7. Detection of hydrogen peroxide (H_2O_2)

The detection process of hydrogen peroxide with N, Zn-CDs as luminescent nano-probe was determined as follows: N, Zn-CDs solution (3 μL) was diluted to 3 mL using aqueous solution of 55 μM Fe^{2+}. The fluorescence intensity of this solution was recorded and defined as F_0. 30 μL of different concentrations of H_2O_2 were added and then the fluorescence intensity of the mixture solution was measured after 5 min and defined as F_1. The relationship between the change of fluorescence intensity ΔF ($\Delta F = F_0 - F_1$) with time and the concentration of H_2O_2 was also plotted.

3. Results and discussion

3.1. Optimization of synthesis conditions

In this work, before optimizing CDs with zinc doping, we have optimized the control CDs i.e. CDs prepared from citric acid and tris(hydroxymethyl)aminomethane. The luminescence property of the CDs was affected by different factors such as the precursors' ratio, hydrothermal temperature. Therefore, in order to achieve CDs with excellent fluorescence properties, experimental conditions need to be optimized. All the reaction parameters were controlled to obtain optimal values. The precursor ratio was found to be the pivotal parameter from different control experiments conducted that influences the photo-physical properties of the CDs and thus was analyzed first. The citric acid concentration was fixed to be 0.1 M, as the carbon source. The ratio of the nitrogen source (tris(hydroxymethyl)aminomethane) and carbon source (citric acid) was varied via alteration of the concentration of (tris (hydroxymethyl)aminomethane). It was observed that the optimum ratio of nitrogen source to carbon source was 3 (Fig. S1a). There was a significant decrease in fluorescence quantum yield (FLQY) when the ratio of nitrogen source and carbon source increased above or decreased below 3. The hydrothermal temperatures examined in this study were 160, 180, 200, 220 and 240 °C keeping the nitrogen source to carbon source as 1:3. The outcome clearly illustrated (Fig. S1b) that FLQY value increases gradually with increasing temperature up to 200 °C, afterward a fall was found for further temperatures. In this whole procedure the hydrothermal reaction time was considered to be 4 h. The optimal experimental conditions were as follow: 0.1 M citric acid, 0.3 M tris(hydroxymethyl)aminomethane, and 200 °C. By maintaining the above conditions we get the control CDs with good fluorescence property (FLQY 45.6%). Now to obtain nitrogen and zinc co-doped CDs (N, Zn-CDs) the control CDs and zinc acetate were chosen as precursor and passivating agents. Moreover to get high quality heteroatom doped CDs (N, Zn-CDs) the FLQY of these CDs was modulated by (i) molar ratio of the precursor and passivating agent used (ii) reaction temperature of the hydrothermal method (iii) time span of the reaction. After maintaining the hydrothermal reaction time and temperature at 4 h and 200 °C respectively, the ratio between control CDs and zinc acetate was varied from 0.1 to 1.2. Fig. 1a describes the change in FLQY with the change of precursor ratio. The highest FLQY was procured at a ratio of 0.5 between control CDs and zinc acetate. When the control CDs and zinc acetate ratio was increased above or decreased below the critical value, FLQY of N, Zn-CDs dropped which indicates the change in chemical composition of the CDs. Hence the ratio of 0.5 between control CDs and zinc acetate was fixed as optimum.

Following the optimal precursor ratio, the hydrothermal reaction temperature, another vital parameter, was regulated to realize the influence of temperature on the FLQY performance of N, Zn-CDs. The hydrothermal reaction temperature was varied from 160 °C to 240 °C (160, 180, 200, 220 and 240 °C) maintaining the reactant molar ratio and reaction time as 0.5 and 4 h constant. Fig. 1b illustrates the correlation between reaction temperature and FLQY of the N, Zn-CDs. The highest FLQY (50.8%) was achieved when the reaction temperature was 200 °C.

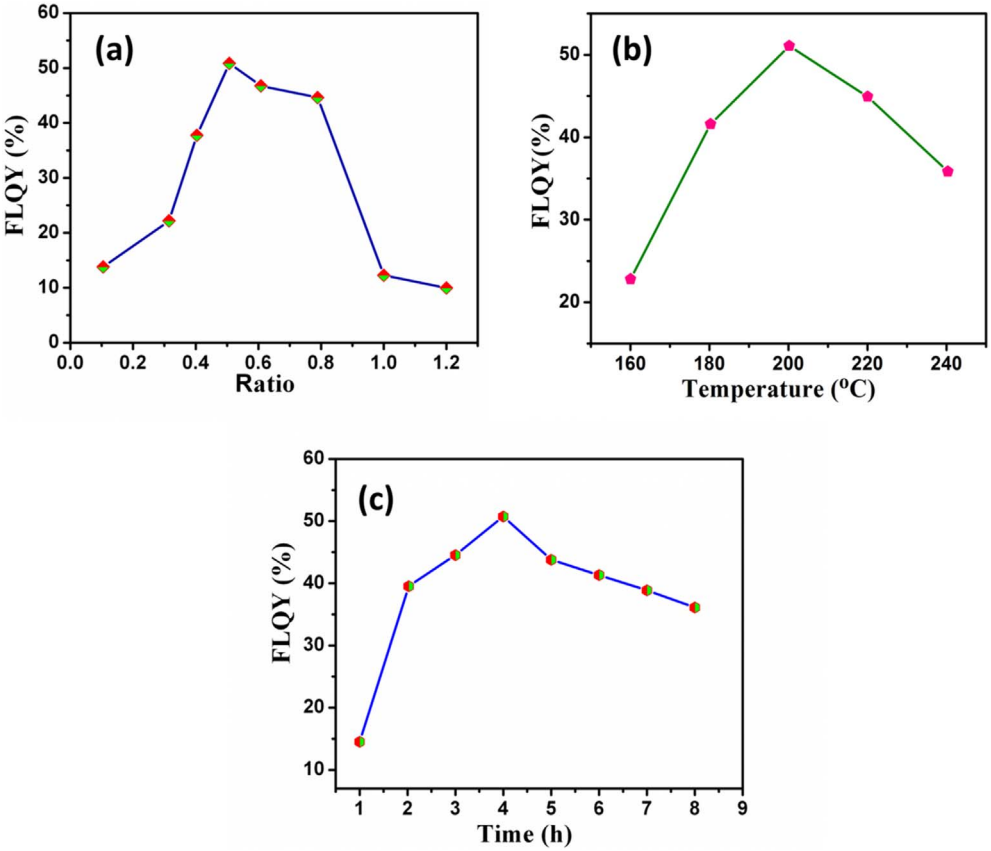

Figure 1. Quantum yield results by (a) molar ratio (b) temperature of the hydrothermal reaction (from 160 to 240 °C); (c) hydrothermal reaction time (from 1 to 8 h).

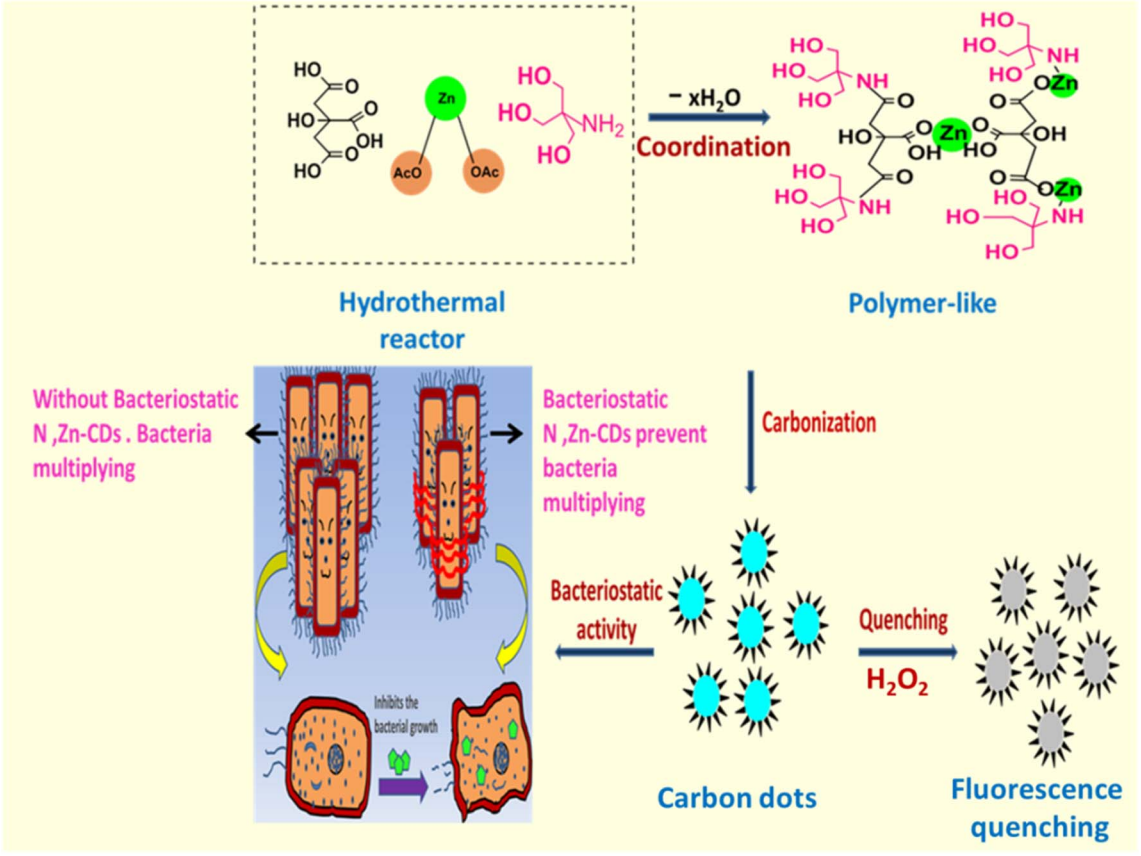

Scheme 1. Schematic approach used to prepare N, Zn-CDs and dual application for bacteriostatic agent against *E. coli* bacteria and Fenton based bio-sensor.

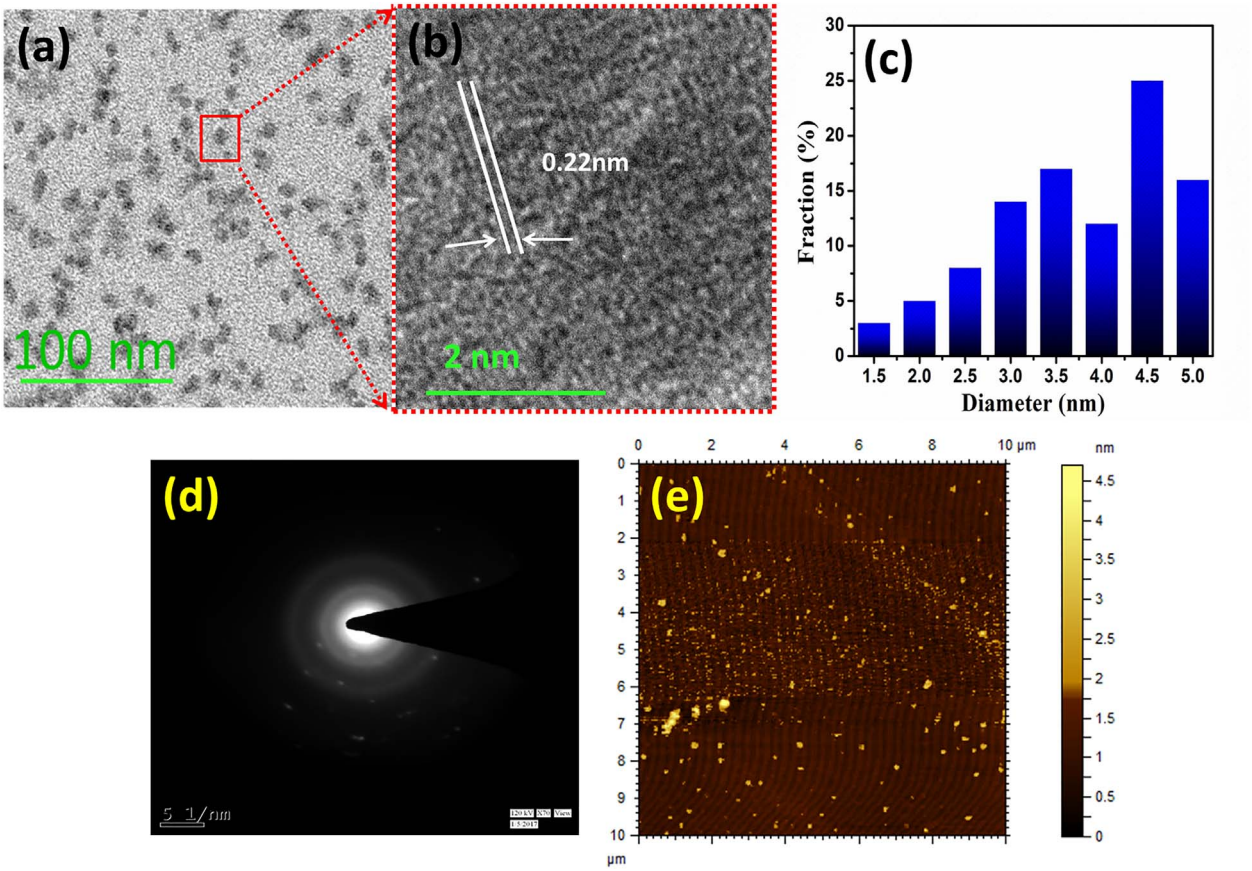

Fig. 2. (a) TEM image of the N, Zn-CDs. (b) High-resolution TEM image of N, Zn-CDs. Lines and arrows indicate the lattice plane distances. (c) Size distribution of the N, Zn-CDs. (d) AFM image of N, Zn-CDs.

Endmost, the influence of reaction time was investigated keeping reaction temperature and precursor molar ratio 200 °C and 0.5 constant, respectively. Fig. 1c clearly indicates that reaction time had pronounced effect on the FLQY of N, Zn-CDs. 4 h reaction time yields with excellent FL properties. Therefore, through different control reactions, the optimal experimental conditions were as follows: precursor molar ratio was 0.5 (0.05 M zinc acetate and 0.1 M control CDs), reaction temperature at 200 °C and reaction time of 4 h. Under these conditions, efficient N and Zn doping occur to generate robust N, Zn-CDs with superior FLQY (50.8%). The schematic approach used to prepare N, Zn-CDs and its dualapplication for bacteriostatic agent against *E. coli* bacteria and Fenton based bio-sensor was represented in Scheme 1.

3.2. Characterizations of as-synthesized CDs

3.2.1. Morphology and analysis of structural properties of N, Zn-CD nanoparticles

The TEM images (Fig. 2a) of the as-prepared N, Zn-CDs reveal that they are spherically small particles and are well separated having relatively narrow size distribution. The HRTEM image (Fig. 2b) of one nano-dot unveils that the graphitic layers have interlayer separation of about 0.22 nm. The statistical particle size distribution of the N, Zn-CDs indicates that they have size ranges from 1.5–5 nm (Fig. 2c), with average diameters of 4.5 nm (100 random particles were analyzed). The AFM topographic image (Fig. 2d) of the N, Zn-CDs was recorded on silicon wafer as substrate. The AFM image demonstrates that the N, Zn-CDs are spherical and are well-dispersed. From AFM measurements, the average height of the N, Zn-CDs obtained is about 3 nm.

The elemental compositions of the N, Zn-CDs were analyzed from EDX data and the distribution was monitored by mapping (Fig. S2). The mass and atomic ratios of carbon (C): nitrogen (N): oxygen (O): zinc (Zn) were found to be 45.57: 11.62: 38.50: 4.30 and 53.47: 11.69: 33.91: 0.93, respectively.

The XRD spectrum (Fig. S3) of the N, Zn-CDs exhibit two wide diffraction peaks (2 theta = 24–31 °, 36–48 °), suggesting to highly disordered carbon composed in random fashion [54,55]. The first peak with broadness character appears at around 28.1°. In comparison to the typical peak (002) around 26.5°, the upward shift of the as-prepared CDs can be described as the decrease of ordered sp^2 layers based on the highly defective-carbon structure on the N, Zn-CDs. Such observation also reveals that the N, Zn-CDs have poor crystallinity, which assigned to the existence of oxygenous groups [56]. It is confirmed further by the selected area electron diffraction (SAED) image shown previously. Raman experiment was performed but no obvious features were obtained. This is because of very high fluorescence property of the N, Zn-CDs which governs over the raman signal [57,58].

The different kind of functional linkages and oxygenated functional groups on the N, Zn-CDs were evident by FTIR data (Fig. 3a). Stretching frequencies at 3573 cm^{-1}, 1724 cm^{-1} and 1100 cm^{-1} were assigned to hydroxyl group (–OH), carbonyl group (C = O) and asymmetric stretching vibrations of C—N, respectively. Peaks obtained at 2950, 1582, 1399 and 1222 cm^{-1} were ascribed the presence of —C—H, C═C, C—O—C and C—O stretching vibrations, respectively. The strong peak of the Zn—O bands near 760 cm^{-1} and 450 cm^{-1} indicates that oxygen formed complexes with the metal. In contrast to the FTIR spectra of the zinc doped CDs (N, Zn-CDs) with control CDs (undoped), the intensities of the zinc doped CDs characteristic peaks at 1724 cm^{-1} (C═O) and 3573 cm^{-1} (—OH) were found to be decreased. The existence of these polar functional groups indicates that the as-prepared N, Zn-CDs have excellent water solubility. The ^1H NMR spectrum of the N, Zn-CDs (Fig. 3b) was analyzed in D_2O which discloses signals in different

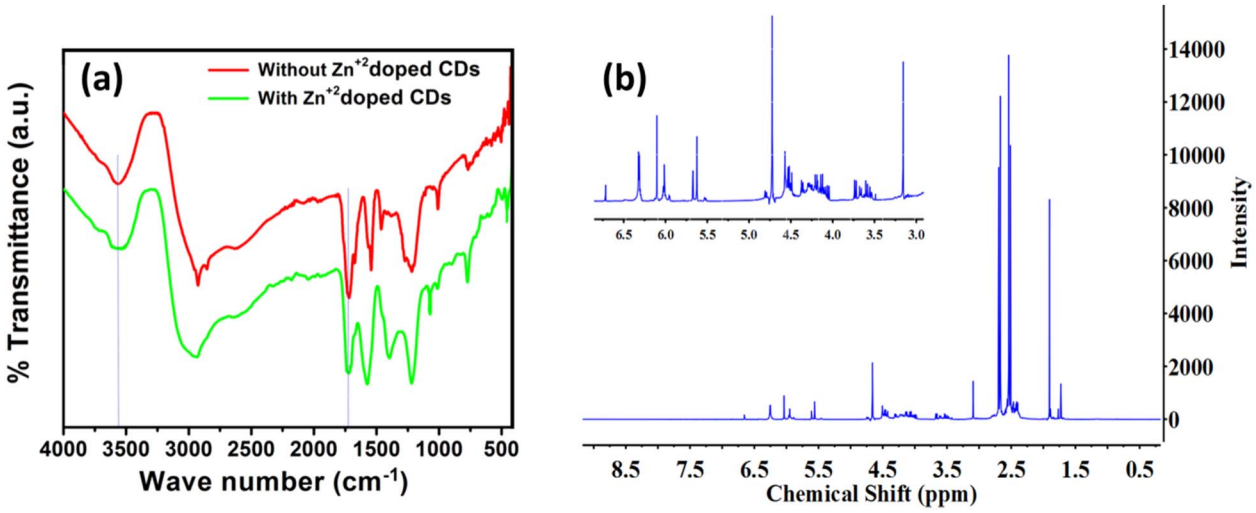

Fig. 3. (a) FTIR spectrum (b) NMR of the N, Zn-CDs.

chemical environments. Peaks in the region 1.6–3 ppm for sp^3 C—H protons and protons of the amine groups, 3–6.5 ppm for the protons attached with carbonyl, hydroxyl and ether groups [59].

To investigate the surface chemical properties, material compositions and bonding within the N, Zn-CDs nano-particles, XPS technique was employed as a characterizing tool. Successful formation nitrogen and zinc doped carbon dots as well as their bonding states are depicted in Fig. 4. Fig. 4a shows a comparison of the survey spectra for clean and as grown carbon dots surface. Both spectra appear with strong existence of C 1s (285 eV), N1s (399 eV), Zn 2p (1023 eV, 1047 eV), and O1s (532 eV) core level binding energy peaks. All these findings confirm the successful formation of N and Zn doped CDs nano-particles. The sputter cleaning leads to a drastic increase in the Zn2p binding energy peaks whereas a significant decrease in the O1s peak, as can be seen in Fig. 4a. However, a strong existence of O1s peak even after the sputter cleaning also indicates the chemical bond formation of O atoms with the bulk N, Zn-CDs rather that a simpler surface contamination.

High resolution scans of C 1s and N 1s core level spectra for sputtered clean N, Zn-CDs surface are shown in Fig. 4b and c, respectively, with various deconvolution components. The deconvoluted C 1s binding energy spectrum is fitted into four peaks at around 284.7 eV, 286.3 eV, 288.1 eV and 289.1 eV, which can be attributed to C—C, C—N (or C—O), C═N and C═O, respectively (Fig. 4b) [60]. Similarly, the N 1 s BE spectrum of N, Zn-CDs is also deconvoluted into two main peaks centering around 401.6 eV and 399.3 eV, corresponding to the N bonded with O and C atoms, respectively (Fig. 4c). These findings can easily be explained in terms of relatively lower and higher electronegativities of C and O with respect that of the N. High resolution Zn2p binding energy spectrum of the N, Zn-CDs surface is presented in Fig. 4d. Two binding energy peaks, positioned at 1023.7 and 1046.9 eV, appear with an energy separation was 23.2 eV and an intensity ratio of 0.52 represent the spin orbit splitting of Zn2p core levels of $Zn2p_{3/2}$ and $Zn2p_{1/2}$, respectively. However, both the peaks appear with a little shift towards the higher binding energy values as compared to the earlier reports [61]. For better clarity and understanding of these peak shifts, a closer look of the $Zn2p_{3/2}$ high resolution spectrum is further analyzed in Fig. 4e, with better statics and deconvolution components. Deconvolution data mainly appears with two sets of $Zn2p_{3/2}$ peaks centered at 1022.4 eV and 1026 eV corresponds to the metallic Zn (0) state of $Zn2p_{3/2}$ and charge transferred satellite state of $Zn2p_{3/2}$, respectively. This observation is consistent with the exchange of electrons between $3d^9$ and $3d^{10}$ orbitals, reported by *Chen* et al. [62] In addition, a partial electron transfer from metallic Zn atoms to the inorganic O atoms as well as chemical bond formation have also to be taken into account. Every detail of all the deconvoluted spectra is summarized for better understanding, as can be seen in Table S1.

The zeta potential of the N, Zn-CDs was tested to be −5.6 eV which can be assigned to the existence of the above functional groups and also confirms the electrostatic stabilization of the N, Zn-CDs aqueous solution. In the meantime, to examine the stability of N, Zn-CDs, they were dispersed in different aqueous solutions including LB medium, PBS solution, normal saline, and deionized water. Up to 3 months clear solutions without any precipitation were observed (Fig. S4) which indicates that N, Zn-CDs are very stable and can be applicable for biomedical applications. The superior water dispersibility of N, Zn-CDs may be mainly ascribed to the ample hydroxyl groups on the CDs surface.

Thermal analysis demonstrates the amount of the mass loss with gradual increment in temperature under inert atmosphere (here N_2 gas was used as inert environment). TGA of pure N, Zn-CDs is depicted in Fig. S5. The initial weight loss of the carbon dots was observed to be 8–10% in between 150 and 200 °C. This primary weight loss may be due to release of H-bonded water molecules and other types of polar-polar attachment among the functional groups present in the carbon dots. Moreover, a steady mass loss was also noticed up to 500 °C. Such high thermal stability may be attributed to the typical graphitic nature of the carbon dots nanoparticles.

3.2.2. *Optical properties*

A set of optical characterizations were performed for the as synthesized N, Zn-CDs. The UV–vis spectrum (Fig. 5a) shows absorption band centered about 328 nm assigned to n-π* transition of carbonyl (C═O) band. From the application and as well as fundamental viewpoint fluorescence is one of the most enchanting behaviors of CDs. But the origin of this unique property is not well-understood. Depending on emissive trap sites, surface passivation, fluorophores, and edge effects different mechanism have been proposed [31,63]. Surface passivation is the most exciting among all these mechanisms because it can deliver efficient direction to prepare CDs of enhanced fluorescence (FL) intensities. The functionalization or surface passivation of CDs can stabilize via radiative recombination of electrons and holes persuaded by oxidation or reduction reactions, which can provides high quantum yield (QY), according to the passivation mechanism.

The as-prepared N, Zn-CDs exhibits strong tunable fluorescence property. As shown in Fig. 5a the N, Zn-CDs show maximum emission at 510 nm when excited at 390 nm. The aqueous dispersion of the N, Zn-CDs exhibit bluish white fluorescence on exposure of UV light (inset of Fig. 5a) at a low concentration (0.11 mg/mL).

Interestingly, the as prepared N, Zn-CDs displays excitation independent (Fig. 5b) PL behavior, in contrast to the dependence found in

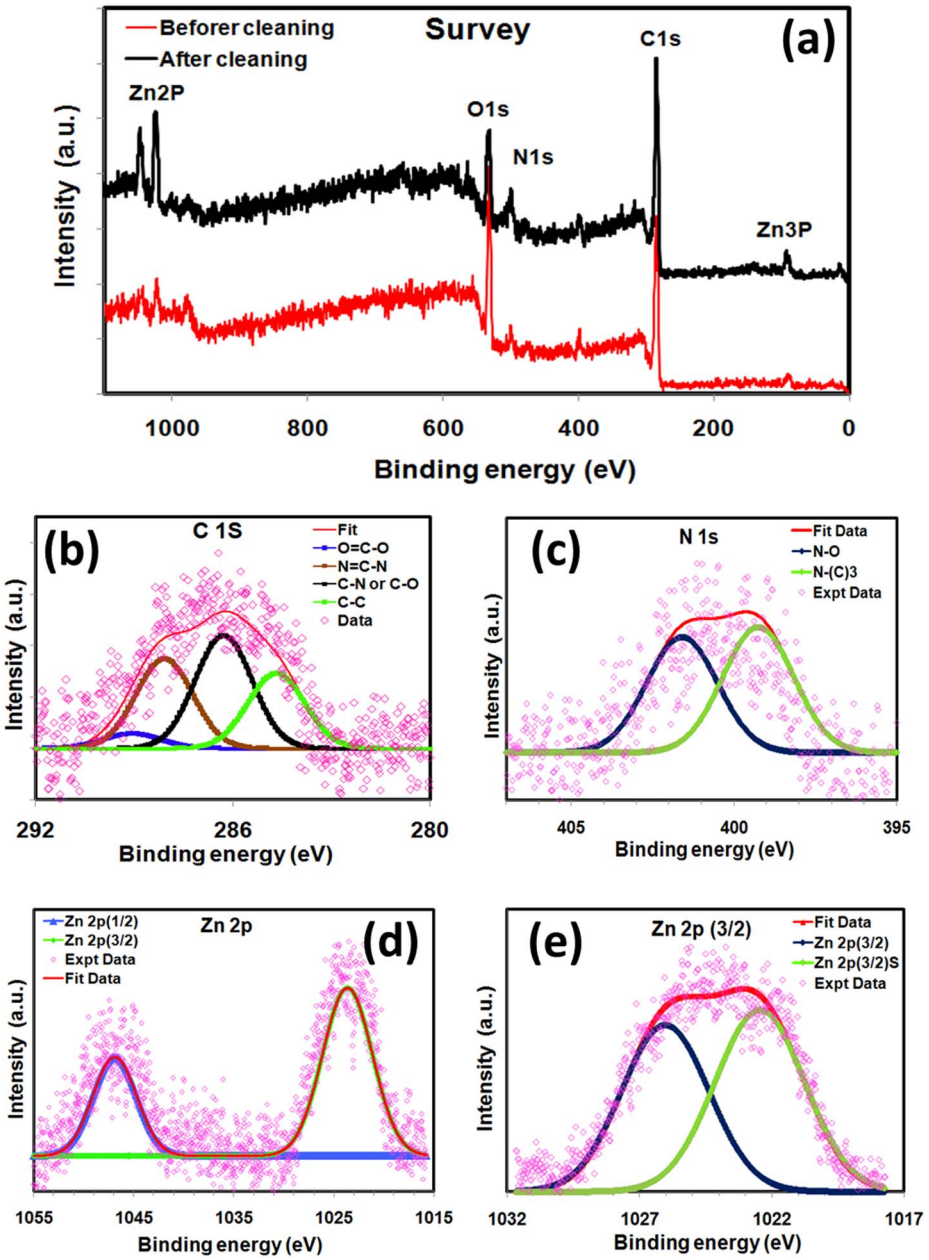

Fig. 4. XPS spectra of (a) wide scan survey of N, Zn CDs nanostructures. High resolution scans of (b) C1s and (c) N1 s spectra (d) Zn2p and (e) Zn2p (3/2) spectra for N, Zn CDs nanostructures, respectively.

other conventional CDs [59,64]. The PL intensity initially increases followed by an attainment of maximum value at the excitation wavelength of 390 nm. After that, a further increment in excitation wavelength from 400 to 440 nm was noticed with gradual lowering of PL intensity without affecting the position of the peak. This distinct property of the N, Zn-CDs is due to Zn doping. The luminescence properties of the Zn doped CDs (N, Zn-CDs) and un-doped CDs (control) were further analyzed. A red shift in the FL signal (Fig. S6) was found compare to the un-doped CDs (control) under identical test condition. A substantial tail was found in the FL response of the un-doped CDs which was showed by most reported CDs. Moreover, the FL decay profiles of the un-doped (Fig. 5c) and Zn doped (Fig. 5d) were investigated. The decay data for both doped and un-doped CDs were well fitted using double-exponential function along with instrument response function. The average FL lifetime of Zn doped and un-doped CDs were found to be 5.9 ns and 4.8 ns, respectively according to the following equation

$$y = A_1 \exp(-x/t_1) + A_2 \exp(-x/t_2) + y_0 \quad (2)$$

The average FL lifetime of Zn doped CDs was larger than the un-doped CDs. The larger FL lifetime of the carbon nanomaterials has been ascribed to passivated defects on the surface of the CDs as excitation energy gap due to inorganic and organic compounds via chemical adsorption or covalent linkages [21]. Due to doping the CDs surface became more passivated as compare to the control. Hence, the doping system shows longer FL lifetime and better FL stability than the control. Using quinine sulfate in 0.1 M H_2SO_4 as a reference, the QY value for the N, Zn-CDs was found to be 50.8% which is higher than the previously reported studies tabulated in Table 1.

The salt effect on the luminescence property of the N, Zn-CDs was examined. From Fig. 5e it can be seen that when KCl concentration remains lower than 0.7 mol/L the FL intensity increases sharply whereas, FL intensity remains almost same as the KCl concentration increases from 0.7–2.0 mol/L. This result assigned to the point that ionic strength of the salt solution significantly regulate the aggregation

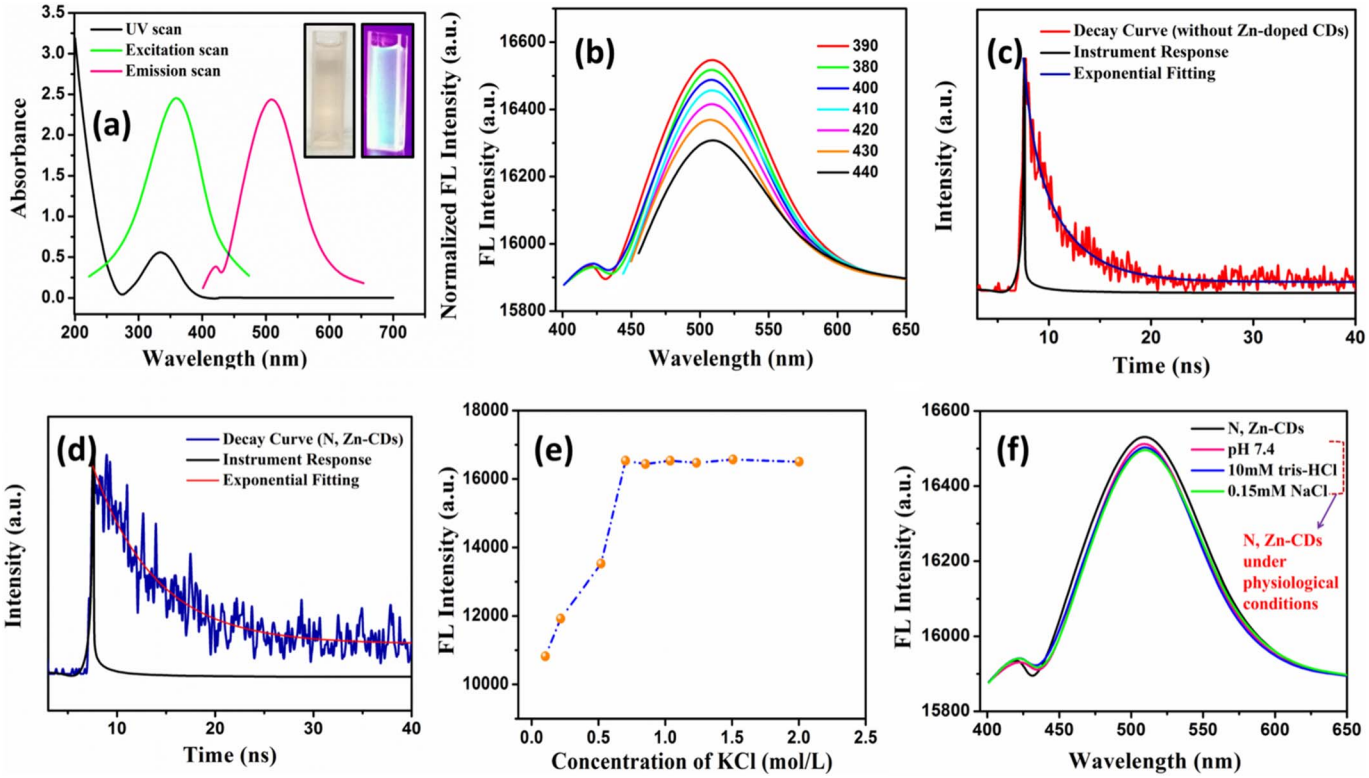

Fig. 5. (a) UV–Vis absorption, excitation and emission spectra of the aqueous dispersion of N, Zn-CDs, inset are photos of N, Zn-CDs under sunlight (left) and irradiated by 365 nm light (right). (b) Excitation independent emission spectra of N, Zn-CDs excited at various wavelengths. (c) FL decay of control CDs. (d) FL decays profile of the N, Zn-CDs. (e) Salt effect of the KCl concentrations on the FL intensity of the N, Zn-CDs. (d) Effect of FL intensity under various physiological conditions.

of the CDs and separate them individually under salt interference. Hence, the as prepared N, Zn-CDs can be applicable under utmost environmental conditions due to strong luminescence property at high salt concentration. Moreover, we analyzed the photostability of the N, Zn-CDs by long term monitoring of FL emission. Fig. S7 shows negligible change of FL intensity at 510 nm under visible light for 18 h. Additionally, even after storage of 60 days no significant change in FL intensity was observed (Fig. S8). Further, we investigate the N, Zn-CDs under different conditions. The luminescence property of N, Zn-CDs scarcely changed by different physiological conditions (Fig. 5f) such as pH 7.4, 10 mM tris-HCl, 0.15 mM NaCl. Fig. S9 displays filter paper impregnated with N, Zn-CDs under sunlight and 365 nm light, respectively. The filter paper shows excellent bluish white luminescence under 365 nm light.

Mostly, two different mechanisms have been proposed to illustrate the FL mechanism of the CDs: emissive traps [21] and electronic conjugate structures [73]. Here, in our study we can inferred that bluish white FL response of the zinc doped CDs originated from the surface passivation of the CDs due to addition of zinc ions. Photoluminescence of the CDs were assigned to radiative recombination of the holes and electrons entrapped at the surface. Inclusion of zinc ions gives rise to new energy levels, resulting in more diverse surface states and red shift of FL signal. Fig. 6 demonstrate the propound energy diagrams for the control CDs and zinc doped CDs. For control CDs, electronic transitions took place between HOMO + I and LUMO, which induce blue luminescence. However, for zinc doped CDs apart from HOMO and HOMO + I level, a new energy level HOMO + II was proposed. This new energy level was supposed to be generated for Zn^{+2}incorporation in CDs. Therefore, for doped CDs electronic transitions could take place from HOMO + II level to LUMO and the excited electrons could relax by radiative recombination. This could be the reason of bluish white emission of zinc doped CDs. The electrons excited from the ground state by absorption of small wavelength (HOMO to LUMO) could get relax through radiative recombination in the HOMO + I and HOMO + II levels. This process results in excitation wavelength independent behavior of the doped CDs.

Based on the above mentioned outcomes, we propose a synthetic mechanism (Fig. 7) of N, Zn-CDs including dehydration, coordination, polymerization, aromatization, nucleation and growth. The coordination between Zn^{2+} and carboxyl or carbonyl groups generated from the

Table 1
Comparison of different types of carbon dots through hydrothermal synthesis.

Temperature (°C)	Time (h)	Fluorescence color	Size (nm)	Reactants	Quantum yield (%)	Reference
200	3	Blue	1.7	Getatin	31.6	[65]
200	3	Blue	2–4	Pomelo peel	6.9	[66]
180	12	Blue	4–7	Chitosan, acetic acid	43	[67]
180	6	Blue-green	3–5	Dopamine	6.4	[68]
300	2	Blue	2.6, 3.3, 3.0, 7.9	Glycine (TRIS, EDTA, cadaverine)	30.6, 26.0, 26.6, 5.4	[69]
120	2.5	Green	1.5–4.5, 50–60	Orange juice, ethanol	25.6, 19.7	[70]
180	3	Blue	13–40	Soy milk	2.6	[71]
160	4	Blue	100, 76	Cellulose (cyclodextrin), NaOH	7.47, 4.49	[72]
200	4	Bluish white	4.5	Citric acid, tris(hydroxymethyl)aminomethane, zinc acetate	50.8	This work

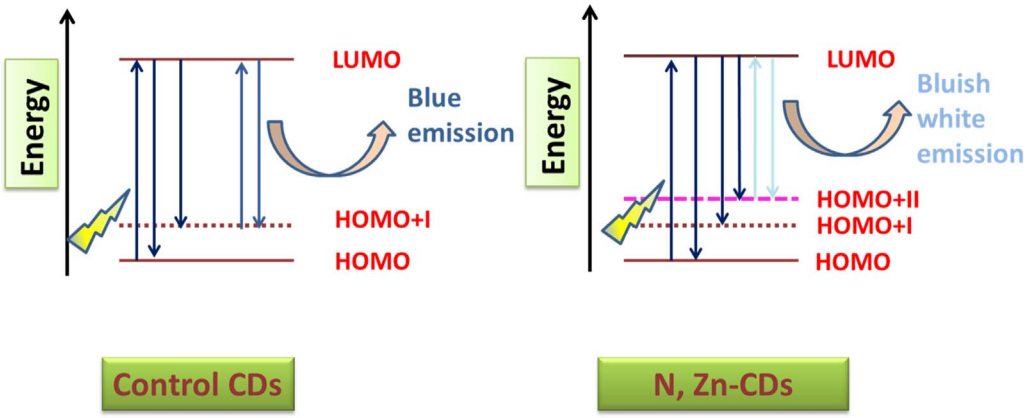

Fig. 6. Schematic illustration of proposed energy levels and electronic transitions of control CDs (left) and N, Zn-CDs (right).

precursor molecules ensued by the dehydration stage [74]. Afterward, the coordinated species undergoes a continuous dehydration process which further leads to large size polymer-like CDs. The polymer-like CDs shrink throughout heating due to continuous intramolecular dehydration. At this stage, a number of C═N and C═C bonds are formed aromatic clusters are generated inside the polymer nanoparticles. When in some local zones of the polymer-like CDs, the concentration of aromatic clusters attains the critical supersaturation point, a burst nucleation of N, Zn-CDs takes place [75]. The so formed nuclei grow up by the high aromatizaton degree of the polymer nanoparticles. Under high temperature with prolonged reaction times, the size and the number of the N, Zn-CDs increase at the cost of sacrificing the polymers. Ultimately, the polymer nanoparticles disappear and only N, Zn-CDs remain.

3.3. Study of bacteriostatic effect of N, Zn-CDs on gram-negative E. coli cells

The as-prepared N, Zn-CDs shows fascinating bacteriostatic behavior. Bacteriostatic material inhibits the bacterial growth and replication of bacteria by interfering with DNA replication, bacterial protein production or other aspects of bacterial cellular metabolism. 100 μL of sterile LB media was mixed with 100 μL of N, Zn-CDs of specified concentration which was inoculated with *E. coli* DH5α cells and incubated overnight at 37 °C. The growth inhibition follows the order as N, Zn-CDs6 (2 mg/mL) > N, Zn-CDs5 (1 mg/mL) > N, Zn-CDs4 (0.5 mg/mL) > N, Zn-CDs3 (0.25 mg/mL) > N, Zn-CDs2 (0.125 mg/mL) > N, Zn-CDs1 (0.062 mg/mL). These concentrations in microtitre plate were shown in Fig. 8a. Herein, the positive control was LB media with bacterial inoculum without addition of N, Zn-CDs and negative control was the media only, no inoculum added, to make sure that no contamination has taken place. From the concentrations in the microtitre plate, we can found at 1 mg/mL no visible growth was observed. Hence, the minimum inhibitory concentration (MIC) was found to be 1 mg/mL for N, Zn-CDs.

On increasing the concentration (0–2 mg/mL) of the N, Zn-CDs, the growth inhibition of *E. coli* increases (Fig. 8b). This result indicates that the concentration of the N, Zn-CDs is a prime parameter for the

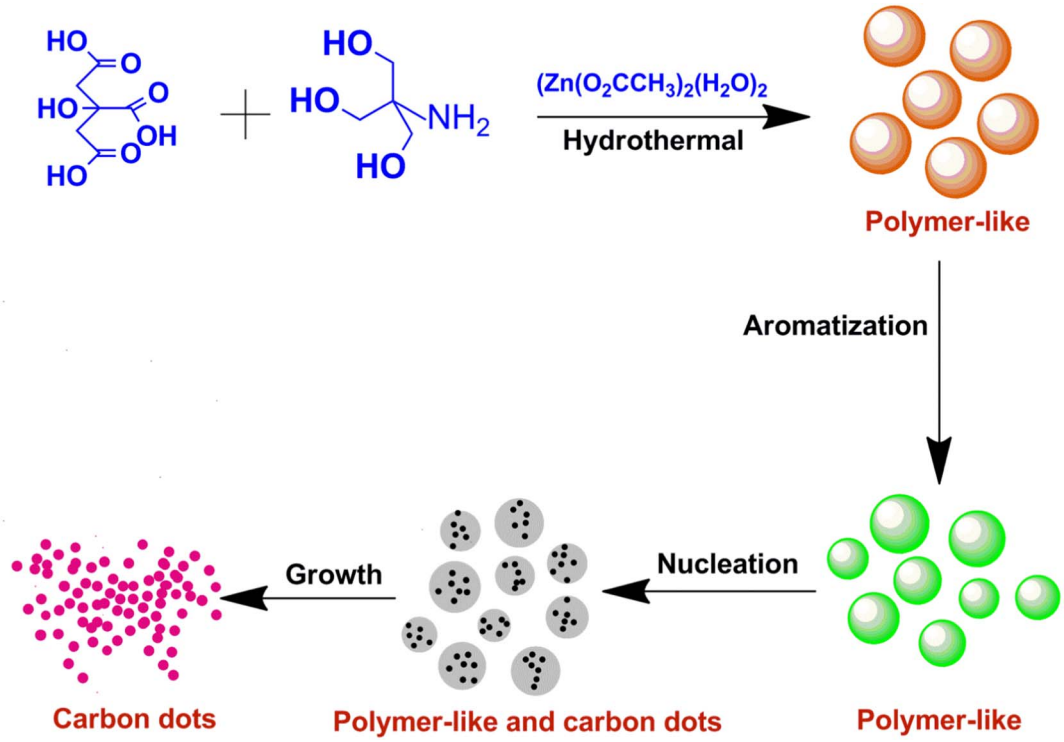

Fig. 7. Schematic representation of the formation mechanism of N, Zn-CDs.

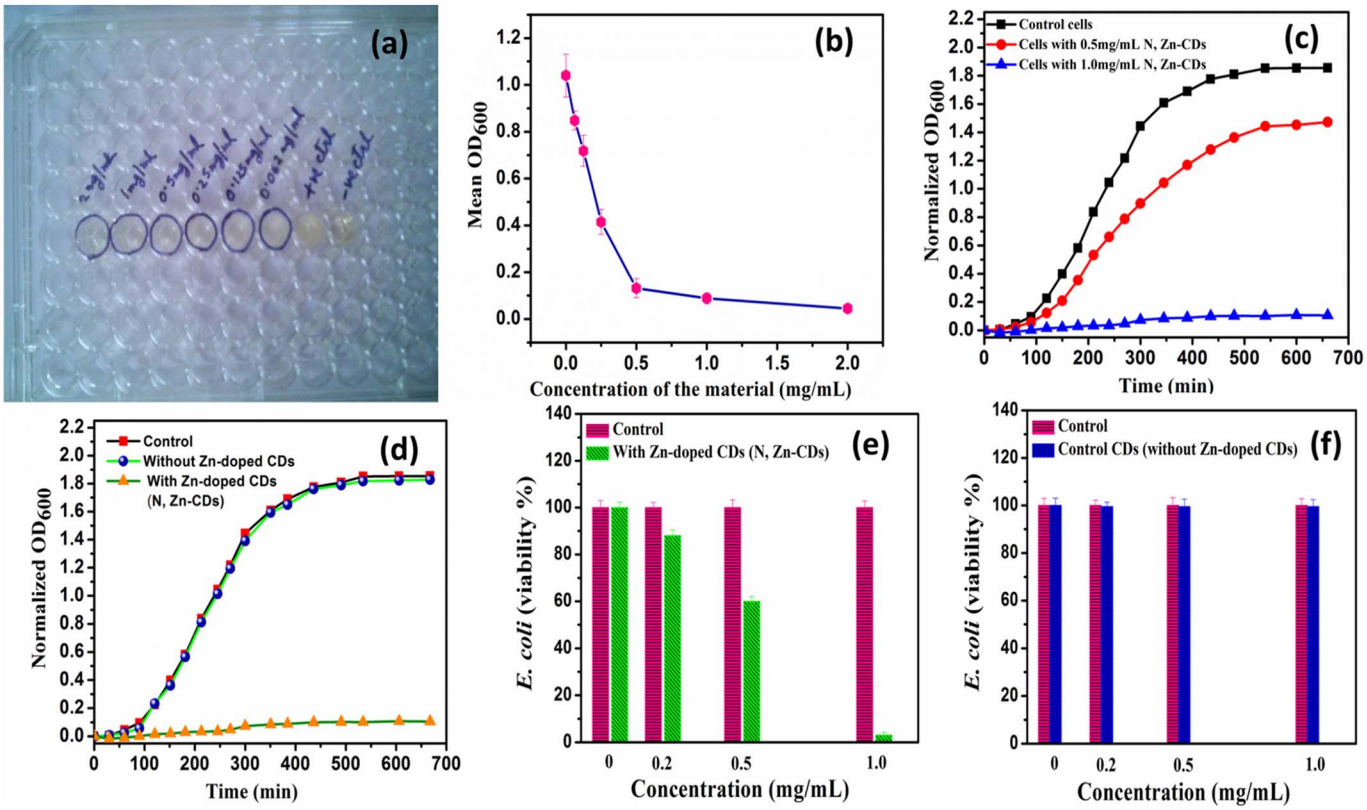

Fig. 8. (a) Microtitre plate image of different concentrations of N, Zn-CDs treated with *E. coli*. (b) Growth inhibition effect of *E. coli* at different concentrations of N, Zn-CDs. (c) Inhibition effect of different concentrations of N, Zn-CDs on the growth of *E. coli* as a function of incubation time. (d) Inhibition effect of N, Zn-CDs and without Zn-doped CDs (control) on the growth of *E. coli* as a function of incubation time at the same concentration of 1 mg/mL. Cell viability evaluation of *E. coli* after treatment with different concentrations of (e) Zn-doped CDs (N, Zn-CDs) and (f) Control CDs.

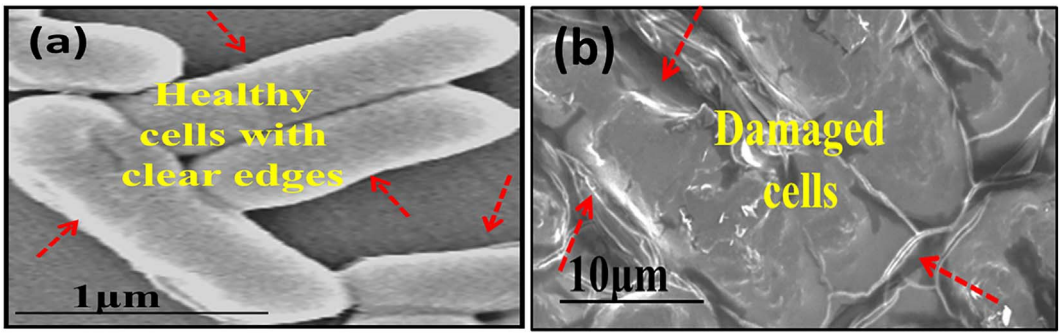

Fig. 9. SEM images of *E. coli* cells (a) without and (b) with the treatment of 1 mg/mL N, Zn-CDs.

bacteriostatic activity. The growth kinetics of gram negative bacteria *E.coli* was monitored in LB broth supplemented with prepared N, Zn-CDs at different conditions. It disclosed that the zero dimensional as-synthesized N, Zn-CDs with different concentrations arrest the growth of *E. coli*. The time dependent bacteriostatic screening was performed by measuring the OD values at 600 nm (OD_{600}) of the bacterial culture supplemented with N, Zn-CDs at different doses. 100 mL of sterile LB media in 3 sets, containing different amount of the N, Zn-CDs (control, 0.5 mg/mL, and 1 mg/mL) were inoculated with the overnight culture of *E. coli* DH5α cells such that the starting OD value is 0.05. It was then incubated in a 37 °C incubator-shaker (200 rpm) and OD at 600 nm was measured at different time intervals.

From Fig. 8c it was observed that when 0.5 mg/mL N, Zn-CDs was used in the media, the bacterial growth was arrested to some extent. The growth of *E. coli* was almost completely inhibited by N, Zn-CDs at a dose of 1 mg/mL. However, when the *E. coli* cells were treated with 1 mg/mL of control CDs (without Zn doping) no growth of inhibition was observed (Fig. 8d). Further, to realize the effect of N, Zn-CDs on *E. coli* DH5α, bacteriological study was carried out by inoculating *E. coli* cells on tryptone soy agar (TSA) plates with different concentrations (0, 0.2, 0.5, 1 mg/mL) of N, Zn-CDs and control CDs (without Zn-doping), incubated overnight at 37 °C. From Fig. 8e it can be seen that N, Zn-CDs exhibits an increasing bacteriostatic activity against *E. coli* DH5α i.e. the bacterial cells were inhibited with increasing concentrations. After the treatment of 1 mg/mL of N, Zn-CDs bacterial colonies were found to be almost inhibited whereas, the viability of control CDs after treatment of same concentrations show (Fig. 8f) no obvious effect on the bacterial cells.

3.3.1. Morphological analysis of E. coli

Bacteriostatic, kind of antimicrobial effects are usually assisted by a change in bacterial surface. In this context, to evaluate the influence of N, Zn-CDs on bacterial cells, the morphological changes of bacteria with and without the treatment of N, Zn-CDs were observed by scanning

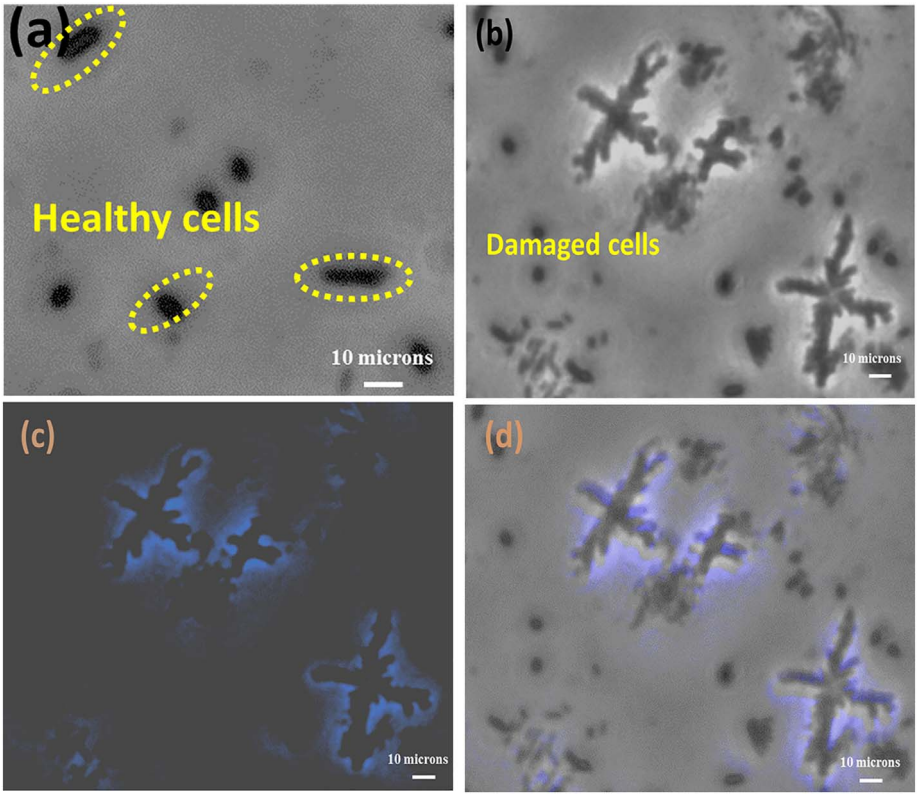

Fig. 10. (a) Bright field images of *E. coli* cells (a) without (b) with the treatment of 1 mg/mL N, Zn-CDs (c) fluorescence image of N, Zn-CDs treated *E. coli* cells taken on exciter filter: excitation 330–385 nm, emission 420 nm (d) merged image of *E. coli* in bright field and fluorescence mode. Scale bar indicates 10 μm. Magnification 40×.

electron microscopy (SEM). As depicted in Fig. 9a *E. coli* cells showed smooth cell walls and clear edges. After the treatment of N, Zn-CDs, cell surfaces became damaged and wrinkled (Fig. 9b). These results suggest that N, Zn-CDs can be potentially used as bacteriostatic agent and the mechanism involved the disruption of bacterial cell walls or membranes.

E. coli cells were also visualized under Olympus (IX51) fluorescence microscope with and without treatment of N, Zn-CDs. Fig. 10a shows the bright field image of the untreated *E. coli*. From the figure healthy cells were clearly observed for untreated *E. coli*. Whereas, damaged and agglomerated bright field image bacterial cells were found when 1 mg/mL N, Zn-CDs was treated with *E. coli* (Fig. 10b). Fig. 10c–d shows the fluorescence microscopic image of *E. coli* (DH5α) under exciter filters in only fluorescence mode and in bright field with fluorescence mode by using N, Zn-CDs, respectively. *E. coli* cells show (Fig. 10c) blue emissions by using N, Zn-CDs (1 mg/mL) as fluorescent imaging probe under exciter filter (excitation 330–385 nm, emission 420 nm) in the fluorescence mode (without bright field). As shown in Fig. 10d we have taken image of bacterial cells under bright field with fluorescence mode by using N, Zn-CDs. These images revealed that N, Zn-CDs can efficiently attach on the bacterial cell surface.

3.4. The special sensitivity of N, Zn-CDs for the hydroxyl radical

Experiment reveals that the N, Zn-CDs are insensitive to hydrogen peroxide. No apparent change in the FL response of the N, Zn-CDs was observed while storing in hydrogen peroxide solution. But, the FL intensity decreases when the solutions containing hydrogen peroxide solution were exposed to UV light. As shown in Fig. S10 the FL intensity of the N, Zn-CDs containing different concentration of hydrogen peroxide solution decreases linearly as the concentration of hydrogen peroxide solution increases. Therefore, it is reasonable to assume that the quenching of the FL intensity causes due to the generation of chemically active species, i.e. hydroxyl radical (·OH) by the UV light irradiation process.

3.5. FL "turn-off" of N, Zn-CDs by Fe^{2+} and H_2O_2

After realizing the pavement of excellent FL, the luminescence property of N, Zn-CDs was investigated for some potential application. The feasibility of sensing H_2O_2 was probed with the aid of Fe^{2+}. The production of ·OH radical from H_2O_2 can be accomplished more easily in the presence of Fe^{2+} ion by Fenton reaction than exposed to UV light. The Fe^{2+} ion reacts with H_2O_2 which could be result in the formation of ·OH radical according to the equation shown below.

$$Fe^{2+} + H_2O_2 \rightarrow Fe^{2+} + {}^{\cdot}OH + OH^{-} \quad (3)$$

Based on the special sensibility of N, Zn-CDs for ·OH radicals and Fenton reaction, the sensing of H_2O_2 is accomplished. Time dependent FL spectrum (from 1 to 10 min) of N, Zn-CDs was studied in the presence of 55 μM H_2O_2 solution. As can be seen from Fig. 11a, no appreciable change of FL intensity was observed indicating that H_2O_2 alone cannot quench the luminescence property of N, Zn-CDs. In the presence of 55 μM Fe^{2+} alone (Fig. 11b) the similar study was analyzed. The result did not present any significant change in FL intensity. But, when simultaneously 55 μM Fe^{2+} and 55 μM H_2O_2 solution were added, the FL response of the N, Zn-CDs reduced significantly. Fig. 11c illustrates rapid decrease of ΔF (change of the FL intensity, $\Delta F = F_0 - F_1$) in the presence of both 55 μM Fe^{2+} and 55 μM H_2O_2 solution within 10 min. The substantial reduction in FL intensity was assigned to the in situ generation of ·OH in the reaction conglomeration. These hydroxyl radicals were generated through the Fenton reaction between Fe^{2+} and H_2O_2. Therefore, this result revealed the usefulness of N, Zn-CDs as fluorescent "turn off" probe for sensing H_2O_2.

3.6. Protocol of optimizing H_2O_2 detection

The optimized experimental conditions were investigated for the

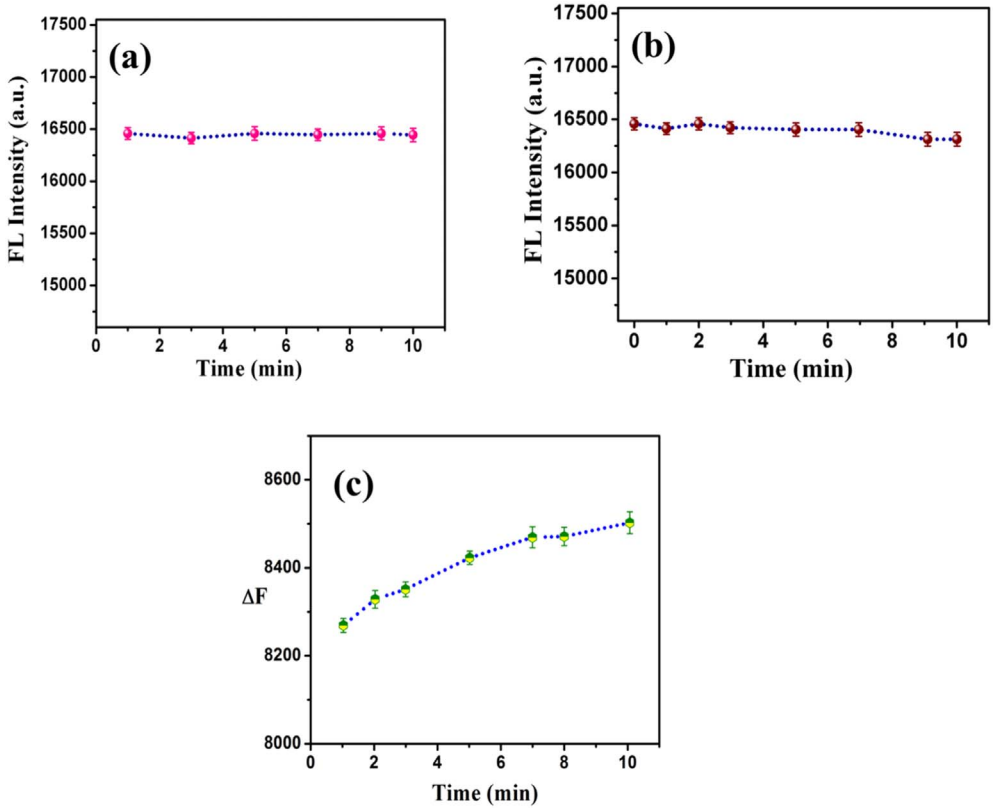

Fig. 11. Time-dependent FL intensity of N, Zn-CDs in (a) 40 μM of Fe^{2+} solution (b) 40 μM H_2O_2 solution, and (c) the degree of diversity (ΔF) of the N, Zn-CDs with change over time in the presence of 40 μM Fe^{2+} and 40 μM H_2O_2 added simultaneously.

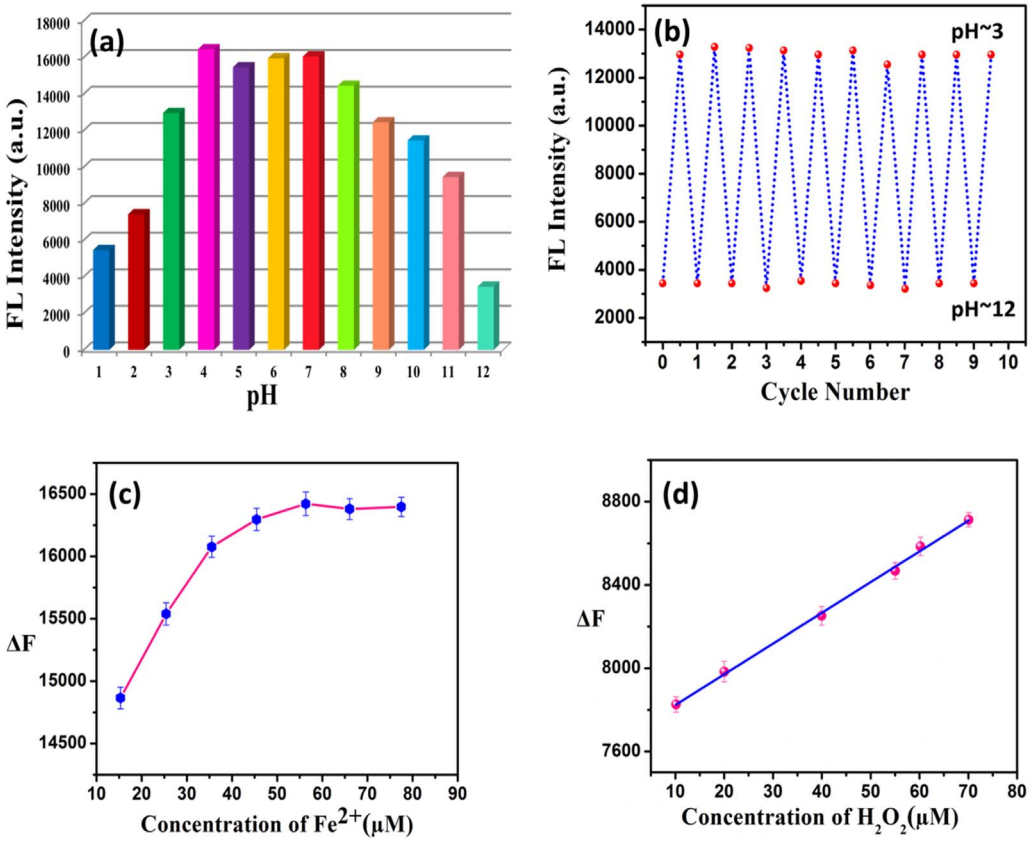

Fig. 12. (a) FL intensity of N, Zn-CDs in different pH values. (b) Reversible behavior of FL intensity upon switching between acidic and basic environments of the N, Zn-CDs (c) Effect of the concentration of Fe^{2+} on the change of FL intensity ΔF (d) change of the FL of N, Zn-CD solution versus the concentration of H_2O_2. Error bars represent the standard deviations of five independent measurements.

Table 2
Comparison of the performance of various hydrogen peroxide sensors.

Materials	Linear range (μM)	Detection limit (μM)	References
MWCNT/PANI	7–2500	2	[77]
CuO	5.0–180	1.6	[78]
PAn-PAA	40–1200	20	[79]
CQDs/octahedral Cu_2O	5–5300	2.8	[80]
Cu_2O–rGOis	100–7800	55.5	[81]
Cu2O MCs	1.5–150	1.5	[82]
N, Zn-CDs	10–70	0.008	This work

detection protocol to serve the enhanced sensitivity of the luminescent probes. To establish the optimized concentration of Fe^{2+} and pH for the detection, the concentration of Fe^{2+} solution and the pH of the buffer solution were varied. At first, the FL signals (Fig. 12a) of N, Zn-CDs in different pH solution (pH range 1 to 12) were analyzed. As can be seen from the result, up to pH 4 gradual increase in FL intensity was noted. However, the N, Zn-CDs illustrates strong and steady FL intensity in the pH range 5 to 8, after which FL intensity decreases gradually. Therefore, the physiological pH (7.4) was chosen as optimal pH for this detection protocol. Furthermore, we studied the reversible behavior of FL intensity upon switching between basic and acidic environments of the N, Zn-CDs. The FL signal decreases when the pH value is changed from 3 to 12 by adding NaOH, and subsequently, when the pH is tuned from 12 to 3 by adding HNO_3, it returns to the initial value. Even after nine cycles no visible perturbation was observed for the pH-switching FL properties of N, Zn-CDs (Fig. 12b) which shows the robust chemical stability of the as-prepared CDs. Hence, it can be said that the reversible behavior of the FL properties at acid and basic conditions is ascribed to the protonation and deprotonation of the N, Zn-CDs.

Afterwards, the impact of the concentration of Fe^{2+} solution on the change of the FL signal (ΔF) was studied (Fig. 12c). Throughout the experiment the concentration of H_2O_2 was fixed to 55 μM. Quenching was maximum when 55 μM Fe^{2+} solution was added, after that ΔF remained almost unchanged. Hence, the optimized conditions for the detection protocol were as follows: pH 7.4 and 55 μM Fe^{2+} solution.

Under the above optimized conditions, the influence of FL intensity of the N, Zn-CDs on the amount of H_2O_2 addition were examined. Fig. 12d displays that as the amount of H_2O_2 increases the FL intensity gradually decreases. A good linear correlation was obtained between the concentration of H_2O_2 (over the range 10–70 μM) and ΔF with a goodness of fit value of 0.99836. In this rapid and sensitive process an ultra-low limit of detection (8 nM) was found using three times standard deviation rule (LOD = 3σ/s, where σ is the standard deviation and s is the slope of the calibration curve). It is worth mentioning that this detection limit is much better than the previous reported studies and is also comparable with the noise level of the previous studies of H_2O_2 detection [76]. A comparison of linear range, detection time for N, Zn-CDs with other hydrogen peroxide sensors reported in the literature was shown in Table 2.

4. Conclusion

In conclusion, we have demonstrated a convenient process for fabricating bluish white luminescent heteroatom doped CDs (N, Zn-CDs). The method is facile and different types of doping can be done to get different kind of CDs. The as-prepared N, Zn-CDs exhibits excellent bacteriostatic activity against gram-negative bacteria *E. coli*. They can efficiently bind to the bacterial surface and negatively effect on the cellular systems. Moreover, the bacterial survivability and the level of oxidative damage depend on the exposure concentration of the N, Zn-CDs. Also, the N, Zn-CDs has been investigated as an intriguing FL probe for the detection of hydrogen peroxide based on the mechanism of Fenton reaction. These CDs displays sensing activity over a wide concentration range associated with the linear range 10–70 μM with a low detection limit of 8 nM. Hence, N, Zn-CDs can be employed for distinguishing of different substrates like oxygen dependent oxidases which can generate hydrogen peroxide upon catalytic oxidation. Therefore, this work represents a readily adaptable FL-based protocol with enormous prospective for application in chemistry and biology.

Appendix A. Supplementary data

Supplementary data to this article can be found online at https://doi.org/10.1016/j.msec.2018.03.010.

References

[1] G. Zhang, Y. Liao, I. Baker, Surface engineering of core/shell iron/iron oxide nanoparticles from microemulsions for hyperthermia, Mater. Sci. Eng. C 30 (2010) 92–97.
[2] A. Kandamchira, S. Selvam, N. Marimuthu, S.K. Janardhanan, N.N. Fathima, Influence of functionalized nanoparticles on conformational stability of type I collagen for possible biomedical applications, Mater. Sci. Eng. C 33 (2013) 4985–4988.
[3] M.J. Tan, Z.-Y. Hong, M.-H. Chang, C.-C. Liu, H.-F. Cheng, X.J. Loh, C.-H. Chen, C.-D. Liao, K.V. Kong, Metal carbonyl-gold nanoparticle conjugates for highly sensitive SERS detection of organophosphorus pesticides, Biosens. Bioelectron. 96 (2017) 167–172.
[4] S.S. Liow, H. Zhou, S. Sugiarto, S. Guo, M.L.S. Chalasani, N.K. Verma, J. Xu, X.J. Loh, Highly efficient supramolecular aggregation-induced emission-active pseudorotaxane luminogen for functional bioimaging, Biomacromolecules 18 (2017) 886–897.
[5] S.S. Liow, Q. Dou, D. Kai, Z. Li, S. Sugiarto, C.Y.Y. Yu, R.T.K. Kwok, X. Chen, Y.L. Wu, S.T. Ong, Long-term real-time in vivo drug release monitoring with AIE thermogelling polymer, Small 13 (2017).
[6] Q.Q. Dou, C.P. Teng, E. Ye, X.J. Loh, Effective near-infrared photodynamic therapy assisted by upconversion nanoparticles conjugated with photosensitizers, Int. J. Nanomedicine 10 (2015) 419.
[7] E. Ye, M.D. Regulacio, M.S. Bharathi, H. Pan, M. Lin, M. Bosman, K.Y. Win, H. Ramanarayan, S.-Y. Zhang, X.J. Loh, An experimental and theoretical investigation of the anisotropic branching in gold nanocrosses, Nano 8 (2016) 543–552.
[8] C.P. Teng, T. Zhou, E. Ye, S. Liu, L.D. Koh, M. Low, X.J. Loh, K.Y. Win, L. Zhang, M.Y. Han, Effective targeted photothermal ablation of multidrug resistant bacteria and their biofilms with NIR-absorbing gold nanocrosses, Adv. Healthc. Mater. 5 (2016) 2122–2130.
[9] Q. Dou, L. Jiang, D. Kai, C. Owh, X.J. Loh, Bioimaging and biodetection assisted with TTA-UC materials, Drug Discov. Today (2017), http://dx.doi.org/10.1016/j.drudis.2017.04.003.
[10] X.J. Loh, Y.-L. Wu, Cationic star copolymers based on β-cyclodextrins for efficient gene delivery to mouse embryonic stem cell colonies, Chem. Commun. 51 (2015) 10815–10818.
[11] X. Wang, K. Qu, B. Xu, J. Ren, X. Qu, Multicolor luminescent carbon nanoparticles: synthesis, supramolecular assembly with porphyrin, intrinsic peroxidase-like catalytic activity and applications, Nano Res. 4 (2011) 908–920.
[12] P. Das, S. Ganguly, M. Bose, S. Mondal, A.K. Das, S. Banerjee, N.C. Das, A simplistic approach to green future with eco-friendly luminescence carbon dots and their application to fluorescence nano-sensor 'turn-off' probe for selective sensing of copper ions, Mater. Sci. Eng. C 75 (2017) 1456–1464.
[13] T. Kavitha, J.-O. Kim, S. Jang, D.-P. Kim, I.-K. Kang, S.-Y. Park, Multifaceted thermoresponsive poly (*N*-vinylcaprolactam) coupled with carbon dots for biomedical applications, Mater. Sci. Eng. C 61 (2016) 492–498.
[14] X. Hu, X. An, L. Li, Easy synthesis of highly fluorescent carbon dots from albumin and their photoluminescent mechanism and biological imaging applications, Mater. Sci. Eng. C 58 (2016) 730–736.
[15] P. Das, M. Bose, S. Ganguly, S. Mondal, A.K. Das, S. Banerjee, N.C. Das, Green approach to photoluminescent carbon dots for imaging of gram-negative bacteria *Escherichia coli*, Nanotechnology 28 (2017) 195501.
[16] S. Ganguly, P. Das, M. Bose, S. Mondal, A.K. Das, N. Das, Strongly blue-luminescent N-doped carbogenic dots as a tracer metal sensing probe in aqueous medium and its potential activity towards in situ ag-nanoparticle synthesis, Sensors Actuators B Chem. (2017), http://dx.doi.org/10.1016/j.snb.2017.06.068.
[17] P. Suvarnaphaet, C.S. Tiwary, J. Wetcharungsri, S. Porntheeraphat, R. Hoonsawat, P.M. Ajayan, I.-M. Tang, P. Asanithi, Blue photoluminescent carbon nanodots from limeade, Mater. Sci. Eng. C 69 (2016) 914–921.
[18] P. LináChee, X. JunáLoh, Multi-functional fluorescent carbon dots with antibacterial and gene delivery properties, RSC Adv. 5 (2015) 46817–46822.
[19] L. Zhou, Z. Li, Z. Liu, J. Ren, X. Qu, Luminescent carbon dot-gated nanovehicles for pH-triggered intracellular controlled release and imaging, Langmuir 29 (2013) 6396–6403.
[20] S.N. Baker, G.A. Baker, Luminescent carbon nanodots: emergent nanolights, Angew. Chem. Int. Ed. 49 (2010) 6726–6744.
[21] L. Cao, X. Wang, M.J. Meziani, F. Lu, H. Wang, P.G. Luo, Y. Lin, B.A. Harruff, L.M. Veca, D. Murray, Carbon dots for multiphoton bioimaging, J. Am. Chem. Soc. 129 (2007) 11318–11319.
[22] S.-T. Yang, L. Cao, P.G. Luo, F. Lu, X. Wang, H. Wang, M.J. Meziani, Y. Liu, G. Qi, Y.-P. Sun, Carbon dots for optical imaging in vivo, J. Am. Chem. Soc. 131 (2009)

11308–11309.
[23] Y. Dong, R. Wang, G. Li, C. Chen, Y. Chi, G. Chen, Polyamine-functionalized carbon quantum dots as fluorescent probes for selective and sensitive detection of copper ions, Anal. Chem. 84 (2012) 6220–6224.
[24] J. Shen, S. Shang, X. Chen, D. Wang, Y. Cai, Facile synthesis of fluorescence carbon dots from sweet potato for Fe 3+ sensing and cell imaging, Mater. Sci. Eng. C 76 (2017) 856–864.
[25] M. Wu, Y. Wang, W. Wu, C. Hu, X. Wang, J. Zheng, Z. Li, B. Jiang, J. Qiu, Preparation of functionalized water-soluble photoluminescent carbon quantum dots from petroleum coke, Carbon 78 (2014) 480–489.
[26] R. Ye, C. Xiang, J. Lin, Z. Peng, K. Huang, Z. Yan, N.P. Cook, E.L. Samuel, C.-C. Hwang, G. Ruan, Coal as an abundant source of graphene quantum dots, Nat. Commun. 4 (2013).
[27] F. Yan, D. Kong, Y. Luo, Q. Ye, Y. Wang, L. Chen, Carbon nanodots prepared for dopamine and Al 3+ sensing, cellular imaging and logic gate operation, Mater. Sci. Eng. C 68 (2016) 732–738.
[28] L. Mohammadi-Behzad, M.B. Gholivand, M. Shamsipur, K. Gholivand, A. Barati, A. Gholami, Highly sensitive voltammetric sensor based on immobilization of bi-sphosphoramidate-derivative and quantum dots onto multi-walled carbon nanotubes modified gold electrode for the electrocatalytic determination of olanzapine, Mater. Sci. Eng. C 60 (2016) 67–77.
[29] S. Ganguly, P. Das, M. Bose, T.K. Das, S. Mondal, A.K. Das, N.C. Das, Sonochemical green reduction to prepare ag nanoparticles decorated graphene sheets for catalytic performance and antibacterial application, Ultrason. Sonochem. 39 (2017) 577–588.
[30] A. Talib, S. Pandey, M. Thakur, H.-F. Wu, Synthesis of highly fluorescent hydrophobic carbon dots by hot injection method using Paraplast as precursor, Mater. Sci. Eng. C 48 (2015) 700–703.
[31] S.Y. Lim, W. Shen, Z. Gao, Carbon quantum dots and their applications, Chem. Soc. Rev. 44 (2015) 362–381.
[32] Y. Yang, J. Zhang, X. Wu, Y. Fu, H. Wu, S. Guo, Composites of boron-doped carbon nanosheets and iron oxide nanoneedles: fabrication and lithiumion storage performance, Mat. Chem. A 2 (2014) 9111–9117.
[33] Z. Qian, X. Shan, L. Chai, J. Ma, J. Chen, H. Feng, Si-doped carbon quantum dots: a facile and general preparation strategy, bioimaging application, and multifunctional sensor, ACS Appl. Mater. Interfaces 6 (2014) 6797–6805.
[34] D. Sun, R. Ban, P.-H. Zhang, G.-H. Wu, J.-R. Zhang, J.-J. Zhu, Hair fiber as a precursor for synthesizing of sulfur-and nitrogen-co-doped carbon dots with tunable luminescence properties, Carbon 64 (2013) 424–434.
[35] J.P. Paraknowitsch, Y. Zhang, B. Wienert, A. Thomas, Nitrogen- and phosphorus-co-doped carbons with tunable enhanced surface areas promoted by the doping additives, Chem. Commun. 49 (2013) 1208–1210.
[36] S. Zhu, Q. Meng, L. Wang, J. Zhang, Y. Song, H. Jin, K. Zhang, H. Sun, H. Wang, B. Yang, Highly photoluminescent carbon dots for multicolor patterning, sensors, and bioimaging, Angew. Chem. Int. Ed. 52 (2013) 3953–3957.
[37] Q. Xu, P. Pu, J. Zhao, C. Dong, C. Gao, Y. Chen, J. Chen, Y. Liu, H. Zhou, Preparation of highly photoluminescent sulfur-doped carbon dots for Fe (III) detection, J. Mater. Chem. A 3 (2015) 542–546.
[38] M.K. Barman, B. Jana, S. Bhattacharyya, A. Patra, Photophysical properties of doped carbon dots (N, P, and B) and their influence on electron/hole transfer in carbon dots–nickel (II) phthalocyanine conjugates, J. Phys. Chem. C 118 (2014) 20034–20041.
[39] J. Zhou, X. Shan, J. Ma, Y. Gu, Z. Qian, J. Chen, H. Feng, Facile synthesis of P-doped carbon quantum dots with highly efficient photoluminescence, RSC Adv. 4 (2014) 5465–5468.
[40] Y. Dong, H. Pang, H.B. Yang, C. Guo, J. Shao, Y. Chi, C.M. Li, T. Yu, Carbon-based dots co-doped with nitrogen and sulfur for high quantum yield and excitation-independent emission, Angew. Chem. Int. Ed. 52 (2013) 7800–7804.
[41] W. Wu, L. Zhan, W. Fan, J. Song, X. Li, Z. Li, R. Wang, J. Zhang, J. Zheng, M. Wu, Cu–N dopants boost electron transfer and photooxidation reactions of carbon dots, Angew. Chem. 127 (2015) 6640–6644.
[42] D.-Y. Guo, C.-X. Shan, S.-N. Qu, D.-Z. Shen, Highly sensitive ultraviolet photodetectors fabricated from ZnO quantum dots/carbon nanodots hybrid films, Sci. Rep. 4 (2014).
[43] Y. Li, B.-P. Zhang, J.-X. Zhao, Z.-H. Ge, X.-K. Zhao, L. Zou, ZnO/carbon quantum dots heterostructure with enhanced photocatalytic properties, Appl. Surf. Sci. 279 (2013) 367–373.
[44] Y. Cheng, B. Li, L. Wang, D. Wei, Y. Feng, D. Jia, Fluorescent zinc doped carbon nanodots derived from chitosan/metal ions complex for cell imaging, Nanomedicine 12 (2016) 506–507.
[45] R. Brayner, R. Ferrari-Iliou, N. Brivois, S. Djediat, M.F. Benedetti, F. Fiévet, Toxicological impact studies based on *Escherichia coli* bacteria in ultrafine ZnO nanoparticles colloidal medium, Nano Lett. 6 (2006) 866–870.
[46] J. Sawai, Quantitative evaluation of antibacterial activities of metallic oxide powders (ZnO, MgO and CaO) by conductimetric assay, J. Microbiol. Methods 54 (2003) 177–182.
[47] N. Jones, B. Ray, K.T. Ranjit, A.C. Manna, Antibacterial activity of ZnO nanoparticle suspensions on a broad spectrum of microorganisms, FEMS Microbiol. Lett. 279 (2008) 71–76.
[48] J. Sawai, T. Yoshikawa, Quantitative evaluation of antifungal activity of metallic oxide powders (MgO, CaO and ZnO) by an indirect conductimetric assay, J. Appl. Microbiol. 96 (2004) 803–809.
[49] N.L. Rosi, C.A. Mirkin, Nanostructures in biodiagnostics, Chem. Rev. 105 (2005) 1547–1562.
[50] A. Thill, O. Zeyons, O. Spalla, F. Chauvat, J. Rose, M. Auffan, A.M. Flank, Cytotoxicity of CeO_2 nanoparticles for *Escherichia coli*. Physico-chemical insight of the cytotoxicity mechanism, Environ. Sci. Technol. 40 (2006) 6151–6156.
[51] P.P. Adiseshaiah, J.B. Hall, S.E. McNeil, Nanomaterial standards for efficacy and toxicity assessment, Wiley Interdiscip. Rev. Nanomed. Nanobiotechnol. 2 (2010) 99–112.
[52] G.A. Crosby, J.N. Demas, Measurement of photoluminescence quantum yields. Review, J. Phys. Chem. 75 (1971) 991–1024.
[53] C. Parker, W. Rees, Fluorescence spectrometry. A review, Analyst 87 (1962) 83–111.
[54] M. Hara, T. Yoshida, A. Takagaki, T. Takata, J.N. Kondo, S. Hayashi, K. Domen, A carbon material as a strong protonic acid, Angew. Chem. Int. Ed. 43 (2004) 2955–2958.
[55] N. Tsubouchi, C. Xu, Y. Ohtsuka, Carbon crystallization during high-temperature pyrolysis of coals and the enhancement by calcium, Energy Fuel 17 (2003) 1119–1125.
[56] J. Peng, W. Gao, B.K. Gupta, Z. Liu, R. Romero-Aburto, L. Ge, L. Song, L.B. Alemany, X. Zhan, G. Gao, Graphene quantum dots derived from carbon fibers, Nano Lett. 12 (2012) 844–849.
[57] A.B. Bourlinos, A. Stassinopoulos, D. Anglos, R. Zboril, M. Karakassides, E.P. Giannelis, Surface functionalized carbogenic quantum dots, Small 4 (2008) 455–458.
[58] F. Wang, M. Kreiter, B. He, S. Pang, C.-y. Liu, Synthesis of direct white-light emitting carbogenic quantum dots, Chem. Commun. 46 (2010) 3309–3311.
[59] B. De, N. Karak, A green and facile approach for the synthesis of water soluble fluorescent carbon dots from banana juice, RSC Adv. 3 (2013) 8286–8290.
[60] P. Fageria, S. Uppala, R. Nazir, S. Gangopadhyay, C.-H. Chang, M. Basu, S. Pande, Synthesis of monometallic (Au and Pd) and bimetallic (AuPd) nanoparticles using carbon nitride (C3N4) quantum dots via the photochemical route for nitrophenol reduction, Langmuir 32 (2016) 10054–10064.
[61] J.-H. Lin, Y.-J. Huang, Y.-P. Su, C.-A. Liu, R.S. Devan, C.-H. Ho, Y.-P. Wang, H.-W. Lee, C.-M. Chang, Y. Liou, Room-temperature wide-range photoluminescence and semiconducting characteristics of two-dimensional pure metallic Zn nanoplates, RSC Adv. 2 (2012) 2123–2127.
[62] L. Chen, M. Hamasaki, H. Manaka, K. Obara, Charge transfer mechanism and spatial density correlation of electronic states of excited zinc (3d 9) films, Open J. Phys. Chem. 2014 (2014).
[63] Y.-P. Sun, B. Zhou, Y. Lin, W. Wang, K.S. Fernando, P. Pathak, M.J. Meziani, B.A. Harruff, X. Wang, H. Wang, Quantum-sized carbon dots for bright and colorful photoluminescence, J. Am. Chem. Soc. 128 (2006) 7756–7757.
[64] M. Xue, Z. Zhan, M. Zou, L. Zhang, S. Zhao, Green synthesis of stable and biocompatible fluorescent carbon dots from peanut shells for multicolor living cell imaging, New J. Chem. 40 (2016) 1698–1703.
[65] Q. Liang, W. Ma, Y. Shi, Z. Li, X. Yang, Easy synthesis of highly fluorescent carbon quantum dots from gelatin and their luminescent properties and applications, Carbon 60 (2013) 421–428.
[66] W. Lu, X. Qin, S. Liu, G. Chang, Y. Zhang, Y. Luo, A.M. Asiri, A.O. Al-Youbi, X. Sun, Economical, green synthesis of fluorescent carbon nanoparticles and their use as probes for sensitive and selective detection of mercury (II) ions, Anal. Chem. 84 (2012) 5351–5357.
[67] Y. Yang, J. Cui, M. Zheng, C. Hu, S. Tan, Y. Xiao, Q. Yang, Y. Liu, One-step synthesis of amino-functionalized fluorescent carbon nanoparticles by hydrothermal carbonization of chitosan, Chem. Commun. 48 (2012) 380–382.
[68] K. Qu, J. Wang, J. Ren, X. Qu, Carbon dots prepared by hydrothermal treatment of dopamine as an effective fluorescent sensing platform for the label-free detection of iron (III) ions and dopamine, Chem. Eur. J. 19 (2013) 7243–7249.
[69] P.-C. Hsu, H.-T. Chang, Synthesis of high-quality carbon nanodots from hydrophilic compounds: role of functional groups, Chem. Commun. 48 (2012) 3984–3986.
[70] S. Sahu, B. Behera, T.K. Maiti, S. Mohapatra, Simple one-step synthesis of highly luminescent carbon dots from orange juice: application as excellent bio-imaging agents, Chem. Commun. 48 (2012) 8835–8837.
[71] C. Zhu, J. Zhai, S. Dong, Bifunctional fluorescent carbon nanodots: green synthesis via soy milk and application as metal-free electrocatalysts for oxygen reduction, Chem. Commun. 48 (2012) 9367–9369.
[72] H. Yan, M. Tan, D. Zhang, F. Cheng, H. Wu, M. Fan, X. Ma, J. Wang, Development of multicolor carbon nanoparticles for cell imaging, Talanta 108 (2013) 59–65.
[73] H. Nie, M. Li, Q. Li, S. Liang, Y. Tan, L. Sheng, W. Shi, S.X.-A. Zhang, Carbon dots with continuously tunable full-color emission and their application in ratiometric pH sensing, Chem. Mater. 26 (2014) 3104–3112.
[74] A.G. Daniel, N.P. Farrell, The dynamics of zinc sites in proteins: electronic basis for coordination sphere expansion at structural sites, Metallomics 6 (2014) 2230–2241.
[75] M. Sevilla, A.B. Fuertes, The production of carbon materials by hydrothermal carbonization of cellulose, Carbon 47 (2009) 2281–2289.
[76] J. Zhang, S.-H. Yu, Carbon dots: large-scale synthesis, sensing and bioimaging, Mater. Today 19 (2016) 382–393.
[77] H. Zhong, R. Yuan, Y. Chai, Y. Zhang, C. Wang, F. Jia, Non-enzymatic hydrogen peroxide amperometric sensor based on a glassy carbon electrode modified with an MWCNT/polyaniline composite film and platinum nanoparticles, Microchim. Acta 176 (2012) 389–395.
[78] L. Zhang, F. Yuan, X. Zhang, L. Yang, Facile synthesis of flower like copper oxide and their application to hydrogen peroxide and nitrite sensing, Chem. Cent. J. 5 (2011) 75.
[79] M.-Y. Hua, C.-J. Chen, H.-C. Chen, R.-Y. Tsai, W. Cheng, C.-L. Cheng, Y.-C. Liu, Preparation of a porous composite film for the fabrication of a hydrogen peroxide sensor, Sensors 11 (2011) 5873–5885.
[80] Y. Li, Y. Zhong, Y. Zhang, W. Weng, S. Li, Carbon quantum dots/octahedral Cu_2O nanocomposites for non-enzymatic glucose and hydrogen peroxide amperometric sensor, Sensors Actuators B Chem. 206 (2015) 735–743.

[81] F. Xu, M. Deng, G. Li, S. Chen, L. Wang, Electrochemical behavior of cuprous oxide–reduced graphene oxide nanocomposites and their application in nonenzymatic hydrogen peroxide sensing, Electrochim. Acta 88 (2013) 59–65.

[82] L. Zhang, H. Li, Y. Ni, J. Li, K. Liao, G. Zhao, Porous cuprous oxide microcubes for non-enzymatic amperometric hydrogen peroxide and glucose sensing, Electrochem. Commun. 11 (2009) 812–815.